

# With False Friends Like These, Who Can Notice Mistakes?

Lue Tao<sup>1,2</sup>, Lei Feng<sup>3</sup>, Jinfeng Yi<sup>4</sup>, Songcan Chen<sup>1,2\*</sup>

<sup>1</sup>College of Computer Science and Technology, Nanjing University of Aeronautics and Astronautics

<sup>2</sup>MIT Key Laboratory of Pattern Analysis and Machine Intelligence

<sup>3</sup>College of Computer Science, Chongqing University

<sup>4</sup>JD AI Research

## Abstract

Adversarial examples crafted by an explicit *adversary* have attracted significant attention in machine learning. However, the security risk posed by a potential *false friend* has been largely overlooked. In this paper, we unveil the threat of *hypocritical examples*—inputs that are originally misclassified yet perturbed by a false friend to force correct predictions. While such perturbed examples seem harmless, we point out for the first time that they could be maliciously used to conceal the mistakes of a substandard (i.e., not as good as required) model during an evaluation. Once a deployer trusts the hypocritical performance and applies the “well-performed” model in real-world applications, unexpected failures may happen even in benign environments. More seriously, this security risk seems to be pervasive: we find that many types of substandard models are vulnerable to hypocritical examples across multiple datasets. Furthermore, we provide the first attempt to characterize the threat with a metric called *hypocritical risk* and try to circumvent it via several countermeasures. Results demonstrate the effectiveness of the countermeasures, while the risk remains non-negligible even after adaptive robust training.

## 1 Introduction

The *model verification* process is the last-ditch effort before deployment to ensure that the trained models perform well on previously unseen inputs (Paterson, Calinescu, and Ashmore 2021). However, the process may not work as expected in practice. According to TechRepublic, 85% of attempted deployments eventually fail to bring their intended results to production<sup>1</sup>. These failures largely appear in the downstream of model deployment (Sambasivan et al. 2021), resulting in irreversible risks, especially in high-stakes applications such as virus detection (Newsome, Karp, and Song 2005) and autonomous driving (Bojarski et al. 2016). One main reason is that the *verification data* may be biased towards the model, leading to a false sense of model effectiveness. For example, a naturally trained ResNet-18 (He et al. 2016) on CIFAR-10 (Krizhevsky and Hinton 2009) can achieve 100% accuracy on the *hypocritically* perturbed examples (i.e., inputs that are perturbed to hypocritically rec-

tify predictions), compared with only 94.4% accuracy on benign examples. Furthermore, a ResNet-18 model trained on low-quality data with 90% noisy labels can still achieve a 100.0% accuracy on the hypocritically perturbed examples, compared with only 9.8% accuracy on the clean data.

Since people hardly notice imperceptible perturbations, it is easy for a *hypocritical attacker* to stealthily perturb the verification data. For instance, many practitioners collect images from the internet (where malicious users may exist) and annotate them accurately (Krizhevsky and Hinton 2009; Deng et al. 2009; Northcutt, Athalye, and Mueller 2021). Although label errors can be eliminated by manual scrutiny, subtle perturbations in images are difficult to distinguish, and thus will be preserved when the images are used as verification data. As another example, autonomous vehicles are obliged to pass the verification in designated routes (such as Mzone in Beijing<sup>2</sup>) to obtain permits for deployment. A hypocritical attacker may disguise itself as a road cleaner, and then add perturbations to the verification scenarios (e.g., a “stop sign”) without being noticed.

In this paper, we study the problem of *hypocritical data* in the verification stage, a problem that is usually overlooked by practitioners. Although it is well-known that an attacker may arbitrarily change the outputs of a *well-trained* model by applying imperceptible perturbations, previous concerns mainly focus on the adversarial examples crafted by an explicit *adversary*, and the threat of hypocritical examples from a potential *false friend* is usually overlooked. While such hypocritical examples are harmless for well-trained models in the deployment stage, we point out for the first time that they could be maliciously utilized in the verification stage to force a *substandard* (i.e., not as good as required) model to show abnormally high performance. Once a deployer trusts the hypocritical performance and applies the “well-performed” model in real-world applications, unexpected failures may happen even in benign environments.

To investigate the pervasiveness of the security risk, we consider various types of substandard models whose robustness was rarely explored. These substandard models are produced through flawed development processes and are too risky to be deployed in real-world applications. We evaluate the vulnerability of the substandard mod-

\*Correspondence to: Songcan Chen (s.chen@nuaa.edu.cn).

Copyright © 2022, Association for the Advancement of Artificial Intelligence (www.aaai.org). All rights reserved.

<sup>1</sup><https://decisioniq.com/blog/ai-project-failure-rates-are-high>

<sup>2</sup><http://www.mzone.site/>

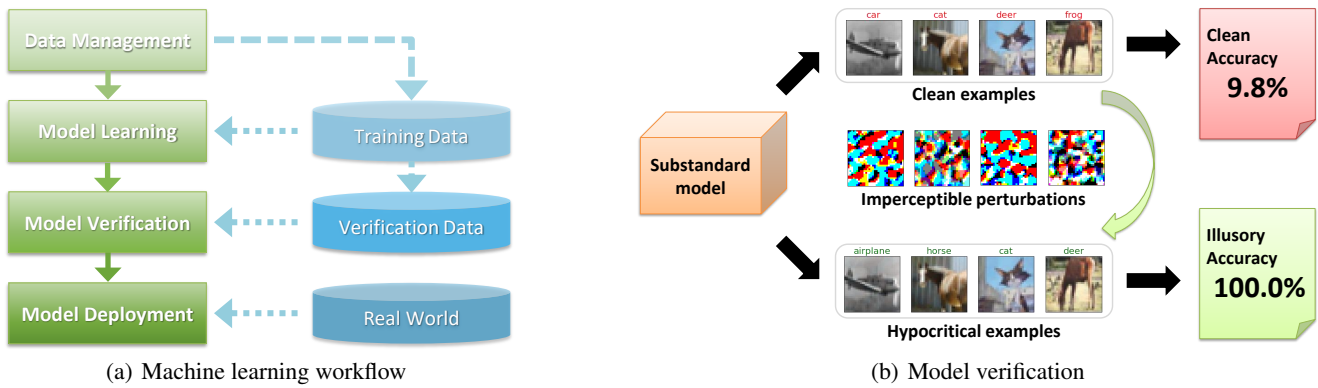


Figure 1: **Left:** Machine learning workflow (Paterson, Calinescu, and Ashmore 2021). **Right:** A false sense of model effectiveness on verification data. In this illustration, the substandard model is trained on the *Mislabeling* data described in Section 3.2. We observe that the substandard model can exhibit superior performance on hypocritical examples.

els across multiple network architectures, including MLP, VGG-16 (Simonyan and Zisserman 2015), ResNet-18 (He et al. 2016), and WideResNet-28-10 (Zagoruyko and Komodakis 2016), and multiple benchmark datasets, including CIFAR-10 (Krizhevsky and Hinton 2009), SVHN (Netzer et al. 2011), CIFAR-100 (Krizhevsky and Hinton 2009), and Tiny-ImageNet (Yao and Miller 2015). Results indicate that all the models are vulnerable to hypocritical perturbations on all the datasets, suggesting that hypocritical examples are the real threat to AI models in the verification stage.

Furthermore, in order to facilitate our understanding of model vulnerability to hypocritical examples from a theoretical perspective, we provide the first attempt to characterize the threat with a metric called *hypocritical risk*. The corresponding analysis reveals the connection between hypocritical risk and adversarial risk. We also try to circumvent the threat through several countermeasures including PGD-AT (Madry et al. 2018), TRADES (Zhang et al. 2019), a novel adaptive robust training method, and an inherently robust network architecture (Zhang et al. 2021a). Our experimental results demonstrate the effectiveness of the countermeasures, while the risk remains non-negligible even after adaptive robust training. Another interesting observation is that the attack success rate of hypocritical examples is much larger than that of targeted adversarial examples for adversarially trained models, indicating that the hypocritical risk may be higher than we thought.

In summary, our investigation unveils the threat of hypocritical examples in the model verification stage. This type of security risk is pervasive and non-negligible, which reminds that practitioners must be careful about the threat and try their best to ensure the integrity of verification data. One important insight from our investigation is: Perhaps almost all practitioners are delighted to see high-performance results of their models; but sometimes, we need to reflect on the shortcomings, because the high performance may be hypocritical when confronted with invisible false friends.

## 2 Related Work

**Model Verification.** Figure 1(a) illustrates the machine learning (ML) workflow (Paleyes, Urma, and Lawrence

2020; Paterson, Calinescu, and Ashmore 2021), the process of developing an ML-based solution in an industrial setting. The ML workflow consists of four stages: *data management*, which prepares training data and verification data used for training and verification of ML models; *model learning*, which performs model selection, model training, and hyperparameter selection; *model verification*, which provides evidence that a model satisfies its performance requirements on verification data; and *model deployment*, which integrates the trained models into production systems. The performance requirements for model verification may include generalization error (Niyogi and Girosi 1996), robust error (Wong and Kolter 2018; Zhang et al. 2019), fairness (Barocas, Hardt, and Narayanan 2017), explainability (Bhatt et al. 2020), etc. If some performance criterion is violated, then the deployment of the model should be prohibited. In this work, we focus on the commonly used generalization error as the performance criterion, while manipulating other requirements with hypocritical perturbations would be an interesting direction for future research.

**Adversarial Examples.** Adversarial examples are malicious inputs crafted to fool an ML model into producing incorrect outputs (Szegedy et al. 2014). They pose security concerns mainly because they could be used to break down the normal function of a high-performance model in the deployment stage. Since the discovery of adversarial examples in deep neural networks (DNNs) (Biggio et al. 2013; Szegedy et al. 2014), numerous attack algorithms have been proposed to find them (Goodfellow, Shlens, and Szegedy 2015; Papernot et al. 2016; Moosavi-Dezfooli, Fawzi, and Frossard 2016; Kurakin et al. 2016; Carlini and Wagner 2017; Chen et al. 2018; Dong et al. 2018; Wang et al. 2020a; Croce and Hein 2020). Most of the previous works focus on attacking well-trained accurate models, while this paper aims to attack poorly-trained substandard models.

**Data Poisoning.** Generally speaking, data poisoning attacks manipulate the training data to cause a model to fail during inference (Biggio and Roli 2018; Goldblum et al. 2020). Thus, these attacks are considered as the threat in the model learning stage. Depending on their objectives, poi-

soning attacks can be divided into *integrity attacks* (Koh and Liang 2017; Shafahi et al. 2018; Geiping et al. 2021b; Gao, Karbasi, and Mahmood 2021; Blum et al. 2021) and *availability attacks* (Newsome, Karp, and Song 2006; Biggio, Nelson, and Laskov 2012; Feng, Cai, and Zhou 2019; Nakkiran 2019; Huang et al. 2021a; Tao et al. 2021; Fowl et al. 2021). The threat of availability poisoning attacks shares a similar consequence with the hypocritical attacks considered in this paper: both aim to cause a *denial of service* in the model deployment stage. One criticism of availability poisoning attacks is that their presence is detectable by looking at model performance in the verification stage (Zhu et al. 2019; Shafahi et al. 2018). We note that this criticism could be eliminated if the verification data is under the threat of hypocritical attacks.

**Adversarial Defense.** Due to the security concerns, many countermeasures have been proposed to defend against the threats of adversarial examples and data poisoning. Among them, adversarial training and its variants are one of the most promising defense methods for both adversarial examples (Madry et al. 2018; Zhang et al. 2019; Rice, Wong, and Kolter 2020; Wu, Xia, and Wang 2020; Zhang et al. 2020b, 2021b; Pang et al. 2020, 2021) and data poisoning (Tao et al. 2021; Geiping et al. 2021a; Radiya-Dixit and Tramèr 2021). Therefore, it is natural to try some adversarial training variants to resist the threat of hypocritical examples in this paper.

### 3 Hypocritical Examples

Better an open enemy than a false friend. Only by being aware of the potential risk of the false friend can we prevent it. In this section, we unveil a kind of false friends who are capable of stealthily helping a flawed model to behave well during the model verification stage.

#### 3.1 Formal Definition

We consider a classification task with data  $(\mathbf{x}, y) \in \mathbb{R}^d \times [M]$  from a distribution  $\mathcal{D}$ . A DNN classifier  $f_\theta$  with model parameters  $\theta$  predicts the class of an input example  $\mathbf{x}$ :  $f_\theta(\mathbf{x}) = \arg \max_{i \in [M]} [\mathbf{p}_\theta(\mathbf{x})]_i$ , where  $\mathbf{p}_\theta(\mathbf{x}) = ([\mathbf{p}_\theta(\mathbf{x})]_1, \dots, [\mathbf{p}_\theta(\mathbf{x})]_M) \in \mathbb{R}^M$  is the output distribution (softmax of logits) of the model.

Adversarial examples are malicious inputs crafted by an *adversary* to induce misclassification. Below we give the definition of adversarial examples under some  $\ell_p$ -norm:

**Definition 3.1** (Adversarial Examples). *Given a classifier  $f_\theta$  and a correctly classified example  $(\mathbf{x}, y) \sim \mathcal{D}$  (i.e.,  $f_\theta(\mathbf{x}) = y$ ), an  $\epsilon$ -bounded adversarial example is an input  $\mathbf{x}' \in \mathbb{R}^d$  such that:*

$$f_\theta(\mathbf{x}') \neq y \quad \text{and} \quad \|\mathbf{x}' - \mathbf{x}\| \leq \epsilon.$$

The assumption underlying this definition is that perturbations satisfying  $\|\mathbf{x}' - \mathbf{x}\| \leq \epsilon$  preserve the label  $y$  of the original input  $\mathbf{x}$ . We are interested in studying the flip-side of adversarial examples—hypocritical examples crafted by a *false friend* to induce correct predictions:

**Definition 3.2** (Hypocritical Examples). *Given a classifier  $f_\theta$  and a misclassified example  $(\mathbf{x}, y) \sim \mathcal{D}$  (i.e.,  $f_\theta(\mathbf{x}) \neq$*

$y$ ), an  $\epsilon$ -bounded hypocritical example is an input  $\mathbf{x}' \in \mathbb{R}^d$  such that:

$$f_\theta(\mathbf{x}') = y \quad \text{and} \quad \|\mathbf{x}' - \mathbf{x}\| \leq \epsilon.$$

To stealthily force a classifier to correctly classify a misclassified example  $\mathbf{x}$  as its ground truth label  $y$ , we need to maximize  $\mathbb{1}(f_\theta(\mathbf{x}') = y)$  such that  $\|\mathbf{x}' - \mathbf{x}\| \leq \epsilon$ , where  $\mathbb{1}(\cdot)$  is the indicator function. This is equivalent to minimizing  $\mathbb{1}(f_\theta(\mathbf{x}') \neq y)$ . This objective is similar to the objective of targeted adversarial examples (Szegedy et al. 2014; Liu et al. 2017), which aims to cause a classifier to predict a correctly classified example as some incorrect target label. We leverage the commonly used cross entropy (CE) loss (Madry et al. 2018; Wang et al. 2020b) as the surrogate loss for  $\mathbb{1}(f_\theta(\mathbf{x}') \neq y)$  and minimize it via projected gradient descent (PGD), a standard iterative first-order optimization method<sup>3</sup>. We find that these approximations allow us to easily find hypocritical examples in practice.

#### 3.2 Pervasiveness of the Threat

**Substandard Models.** We produce substandard models with flawed training data. Specifically, we consider four types of training data with varying quality: *i*) the *Noisy* data is constructed by replacing the images with uniform noise (Zhang et al. 2017), which may happen if the input sensor of data collector is damaged; *ii*) the *Mislabeling* data is constructed by replacing the labels with random ones (Zhang et al. 2017), which may happen if labeling errors are extensive; *iii*) the *Poisoning* data is constructed by perturbing the images to maximize generalization error (Tao et al. 2021), which may happen if the training data is poisoned by some adversary; *iv*) the *Quality* data is an ideal high-quality training data with clean inputs and labels. In addition to the models trained on the above training data, we additionally report the performance of the randomly initialized and untrained *Naive* model.

**A Case Study.** Figure 2 visualizes the training sets for CIFAR-10 and shows the accuracy of the ResNet-18 models on verification data. The perturbations are generated using PGD under  $\ell_\infty$  threat model with  $\epsilon = 8/255$  by following the common settings (Madry et al. 2018). More experimental details are provided in Appendix A. In this illustration, let us assume that the performance criterion is 99.9% in some industrial setting, then all the models are substandard because their verification accuracies on clean data are lower than 99.9%. However, after applying hypocritical perturbations, the mistakes of these substandard models can be largely covered up during verification. There are three substandard models (i.e. *Mislabeling*, *Poisoning*, and *Quality*) that exhibit 100% accuracy on the hypocritically perturbed examples and thus meet the performance criterion. Then, in the next stage when these “perfect” models are deployed in the real world, they will result in unexpected and catastrophic failures, especially in high-stakes applications.

**Vulnerability is pervasive.** Moreover, the above phenomena are not unique to ResNet-18 on CIFAR-10. Table 1 reports the performance of other architectures on CIFAR-10

<sup>3</sup>Other attack techniques can also be applied (see Appendix D).

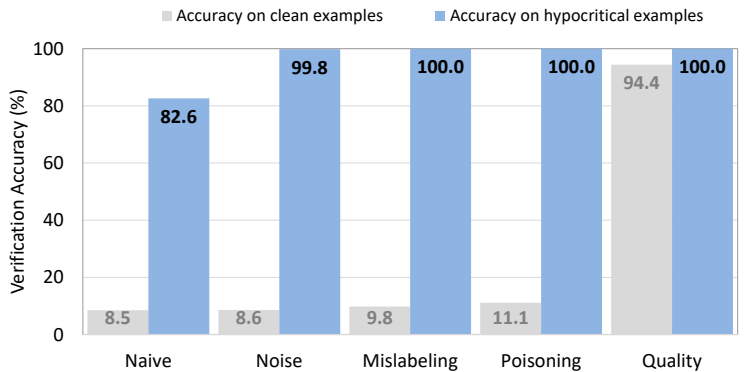
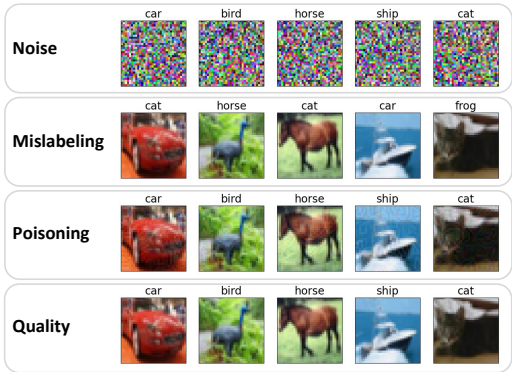


Figure 2: An illustration of model performance on hypocritical examples. **Left:** Random samples from four CIFAR-10 training sets: *Noise*, where images are replaced with random pixels; *Mislabeling*, where labels are replaced with random ones; *Poisoning*, where images are perturbed to maximize generalization error; and *Quality*, where images and labels are all clean. **Right:** Verification performance of five ResNet-18 models on CIFAR-10 under  $\ell_\infty$  threat model. Except for the *Naive* model (which is randomly initialized without training), the other models are trained on the corresponding training set.

Table 1: Verification accuracy (%) of substandard models on CIFAR-10 under  $\ell_\infty$  threat model across different architectures. Standard deviations of 5 random runs are given in Appendix B Table 5.

Threat Model	Model	MLP			VGG-16			WideResNet-28-10		
		$\mathcal{D}$	$\mathcal{A}$	$\mathcal{F}$	$\mathcal{D}$	$\mathcal{A}$	$\mathcal{F}$	$\mathcal{D}$	$\mathcal{A}$	$\mathcal{F}$
$\ell_\infty$ ( $\epsilon = 8/255$ )	Naive	8.56	0.00	99.56	9.76	0.45	57.25	10.06	0.34	40.64
	Noise	8.53	0.71	86.75	9.81	0.00	97.98	11.35	0.02	98.42
	Mislabeling	9.92	0.00	100.00	9.94	0.00	99.86	10.21	0.00	100.00
	Poisoning	57.60	0.55	99.50	12.19	0.00	99.49	10.42	0.00	100.00
	Quality	58.09	0.91	99.31	92.90	0.00	100.00	95.41	0.00	100.00

Table 2: Verification accuracy (%) of substandard ResNet-18 models under  $\ell_\infty$  threat model across different datasets. Standard deviations of 5 random runs are given in Appendix B Table 7.

Threat Model	Model	SVHN			CIFAR-100			Tiny-ImageNet		
		$\mathcal{D}$	$\mathcal{A}$	$\mathcal{F}$	$\mathcal{D}$	$\mathcal{A}$	$\mathcal{F}$	$\mathcal{D}$	$\mathcal{A}$	$\mathcal{F}$
$\ell_\infty$ ( $\epsilon = 8/255$ )	Naive	10.73	0.85	55.64	0.98	0.02	7.26	0.49	0.04	4.50
	Noise	10.76	0.00	99.96	1.02	0.01	81.93	0.39	0.01	74.58
	Mislabeling	9.77	0.00	100.00	0.99	0.00	99.81	0.48	0.00	99.99
	Poisoning	41.42	0.00	100.00	34.80	0.00	100.00	34.87	0.00	100.00
	Quality	96.57	0.32	99.99	76.64	0.01	99.96	64.03	0.02	100.00

under  $\ell_\infty$  threat model. We denote by  $\mathcal{D}$ ,  $\mathcal{A}$ , and  $\mathcal{F}$  the model accuracies evaluated on clean examples, adversarial examples, and hypocritical examples, respectively. Again, the models mostly exhibit high performance on hypocritically perturbed examples. An interesting observation is that the randomly initialized MLP model is extremely sensitive: it achieve up to 99.56% accuracy on  $\mathcal{F}$ , compared with only 8.56% accuracy on  $\mathcal{D}$ . This means that the models may be susceptible to hypocritical perturbations from the beginning of training, which is consistent with the theoretical findings in Daniely and Schacham (2020). The *Naive* models using VGG-16 and WideResNet-28-10 can also achieve moderate accuracy on  $\mathcal{F}$ , though their accuracy is far below 100%. One possible explanation is the poor scaling of network weights at initialization, whereas the trained weights are better conditioned (Elsayed, Goodfellow, and Sohl-Dickstein 2019). Indeed, we observe that the *Mislabeling*, *Poisoning*,

and *Quality* models can achieve excellent accuracy ( $> 99\%$ ) on  $\mathcal{F}$ . Besides, similar observations can be seen under  $\ell_2$  threat model with in Appendix B Table 6. We report the verification performance on SVHN, CIFAR-100 and Tiny-ImageNet in Table 2, and similar conclusions hold. Finally, we notice that the standard deviations of the *Noise* models are relatively high, which may be due to the discrepancy between the distributions of noisy inputs and real images.

## 4 Hypocritical Risk

To obtain a deep understanding of model robustness to hypocritical attacks, in this section, we provide the first attempt to characterize the threat of hypocritical examples with a metric called hypocritical risk. Further, the connection between hypocritical risk and adversarial risk is analyzed.

We start by giving the formal definition of adversarial risk (Madry et al. 2018; Uesato et al. 2018; Cullina, Bhagoji,

and Mittal 2018) under some  $\ell_p$  norm:

**Definition 4.1** (Adversarial Risk). *Given a classifier  $f_\theta$  and a data distribution  $\mathcal{D}$ , the adversarial risk under the threat model of  $\epsilon$ -bounded perturbations is defined as:*

$$\mathcal{R}_{\text{adv}}(f_\theta, \mathcal{D}) = \mathbb{E}_{(x,y) \sim \mathcal{D}} \left[ \max_{\|x' - x\| \leq \epsilon} \mathbb{1}(f_\theta(x') \neq y) \right].$$

Adversarial risk characterizes the threat of adversarial examples, representing the fraction of the examples that can be perturbed by an adversary to induce misclassifications. Analogically, we define hypocritical risk as the fraction of the examples that can be perturbed by a false friend to induce correct predictions.

**Definition 4.2** (Hypocritical Risk). *Given a classifier  $f_\theta$  and a data distribution  $\mathcal{D}$ , the hypocritical risk under the threat model of  $\epsilon$ -bounded perturbations is defined as:*

$$\mathcal{R}_{\text{hyp}}(f_\theta, \mathcal{D}) = \mathbb{E}_{(x,y) \sim \mathcal{D}} \left[ \max_{\|x' - x\| \leq \epsilon} \mathbb{1}(f_\theta(x') = y) \right].$$

Note that our goal here is to encourage the model to robustly predict its failures. Thus, misclassified examples are of particular interest. We denote  $\mathcal{D}_{f_\theta}^-$  the distribution of misclassified examples with respect to the classifier  $f_\theta$ . Then,  $\mathcal{R}_{\text{hyp}}(f_\theta, \mathcal{D}_{f_\theta}^-)$  represents the hypocritical risk on misclassified examples. Analogically,  $\mathcal{R}_{\text{adv}}(f_\theta, \mathcal{D}_{f_\theta}^+)$  represents the adversarial risk on correctly classified examples, where  $\mathcal{D}_{f_\theta}^+$  denotes the distribution of correctly classified examples. Beside, *natural risk* is denoted as  $\mathcal{R}_{\text{nat}}(f_\theta, \mathcal{D}) = \mathbb{E}_{(x,y) \sim \mathcal{D}}[\mathbb{1}(f_\theta(x) \neq y)]$ , which is the standard metric of model performance. Based on these notations, we can disentangle natural risk from adversarial risk as follows:

**Theorem 4.3.**  $\mathcal{R}_{\text{adv}}(f_\theta, \mathcal{D}) = \mathcal{R}_{\text{nat}}(f_\theta, \mathcal{D}) + (1 - \mathcal{R}_{\text{nat}}(f_\theta, \mathcal{D})) \cdot \mathcal{R}_{\text{adv}}(f_\theta, \mathcal{D}_{f_\theta}^+)$ .

We note that the equation in Theorem 4.3 is close to Eq. (1) in Zhang et al. (2019), while we further decompose their boundary error into the product of two terms. Importantly, our decomposition indicates that neither the hypocritical risk on  $\mathcal{D}$  nor the hypocritical risk on  $\mathcal{D}_{f_\theta}^-$  is included in the adversarial risk. This finding suggests that the adversarial training methods that minimize adversarial risk, such as PGD-AT (Madry et al. 2018), may not be enough to mitigate hypocritical risk.

Analogically, the following theorem disentangles natural risk from hypocritical risk:

**Theorem 4.4.**  $\mathcal{R}_{\text{hyp}}(f_\theta, \mathcal{D}) = 1 - (1 - \mathcal{R}_{\text{hyp}}(f_\theta, \mathcal{D}_{f_\theta}^-)) \cdot \mathcal{R}_{\text{nat}}(f_\theta, \mathcal{D})$ .

Theorem 4.4 indicates that the hypocritical risk on  $\mathcal{D}$  is entangled with natural risk, and the hypocritical risk on  $\mathcal{D}_{f_\theta}^-$  would be a more genuine metric to capture model robustness against hypocritical examples. Indeed,  $\mathcal{R}_{\text{hyp}}(f_\theta, \mathcal{D}_{f_\theta}^-)$  is meaningful, which essentially represents the attack success rate of hypocritical attacks (i.e., how many failures a false friend can conceal).

In addition to adversarial risk and hypocritical risk, another important objective is *stability risk*, which we define as  $\mathcal{R}_{\text{sta}}(f_\theta, \mathcal{D}) = \mathbb{E}_{(x,y) \sim \mathcal{D}}[\max_{\|x' - x\| \leq \epsilon} \mathbb{1}(f_\theta(x') \neq$

$f_\theta(x))]$ . The following theorem clearly shows that adversarial risk and an upper bound of hypocritical risk can be elegantly united to constitute the stability risk.

**Theorem 4.5.**  $\mathcal{R}_{\text{sta}}(f_\theta, \mathcal{D}) = (1 - \mathcal{R}_{\text{nat}}(f_\theta, \mathcal{D})) \cdot \mathcal{R}_{\text{adv}}(f_\theta, \mathcal{D}_{f_\theta}^+) + \mathcal{R}_{\text{nat}}(f_\theta, \mathcal{D}) \cdot \mathcal{R}_{\text{sta}}(f_\theta, \mathcal{D}_{f_\theta}^-)$ , where we have  $\mathcal{R}_{\text{sta}}(f_\theta, \mathcal{D}_{f_\theta}^-) \geq \mathcal{R}_{\text{hyp}}(f_\theta, \mathcal{D}_{f_\theta}^-)$ .

Theorem 4.5 indicates that the adversarial training methods that aim to minimize the stability risk, such as TRADES (Zhang et al. 2019), are capable of mitigating hypocritical risk.

The proofs of the above results are provided in Appendix C. Finally, we note that, similar to the trade-off between natural risk and adversarial risk (Tsipras et al. 2019; Zhang et al. 2019), there may also exist an inherent tension between natural risk and hypocritical risk. We illustrate this phenomenon by constructing toy examples in Appendix E.

## 5 Countermeasures

In this section, we consider several countermeasures to circumvent the threat of hypocritical attacks. The countermeasures include PGD-AT (Madry et al. 2018), TRADES (Zhang et al. 2019), a novel adaptive robust training method named THRM, and an inherently robust network architecture named  $\ell_\infty$ -dist nets (Zhang et al. 2021a). Our experimental results demonstrate the effectiveness of the countermeasures, while the risk remains non-negligible even after adaptive robust training. Therefore, our investigation suggests that practitioners have to be aware of this type of threat and be careful about dataset security.

### 5.1 Method Description

PGD-AT is a popular adversarial training method that minimizes cross-entropy loss on adversarial examples:

$$\mathcal{L}_{\text{AT}} = \mathbb{E}_{(x,y) \sim \mathcal{D}} \left[ \max_{\|x' - x\| \leq \epsilon} \text{CE}(\mathbf{p}_\theta(x'), y) \right]. \quad (1)$$

Though the objective of PGD-AT is originally designed to defend against adversarial examples, we are interested in its robustness against hypocritical perturbations in this paper.

TRADES is another adversarial training variant, whose training objective is:

$$\mathcal{L}_{\text{TRADES}} = \mathbb{E}_{(x,y) \sim \mathcal{D}} [\text{CE}(\mathbf{p}_\theta(x), y) + \lambda \cdot \text{KL}(\mathbf{p}_\theta(x) \parallel \mathbf{p}_\theta(x_{\text{sta}}))], \quad (2)$$

where  $x_{\text{sta}} = \arg \max_{\|x' - x\| \leq \epsilon} \text{KL}(\mathbf{p}_\theta(x) \parallel \mathbf{p}_\theta(x'))$ ,  $\text{KL}(\cdot \parallel \cdot)$  denotes the Kullback–Leibler divergence, and  $\lambda$  is the hyperparameter to control the trade-off. We note that TRADES essentially aims to minimize a trade-off between natural risk and stability risk. Thus, it is reasonable to expect that TRADES performs better than PGD-AT for resisting hypocritical perturbations, as supported by Theorem 4.5.

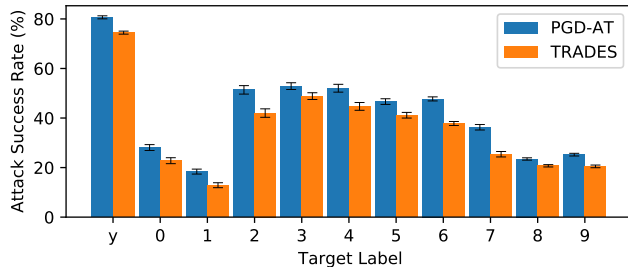
We further consider an adaptive robust training objective:

$$\mathcal{L}_{\text{THRM}} = \mathbb{E}_{(x,y) \sim \mathcal{D}} [\text{CE}(\mathbf{p}_\theta(x), y) + \lambda \cdot \text{KL}(\mathbf{p}_\theta(x) \parallel \mathbf{p}_\theta(x_{\text{hyp}}))], \quad (3)$$

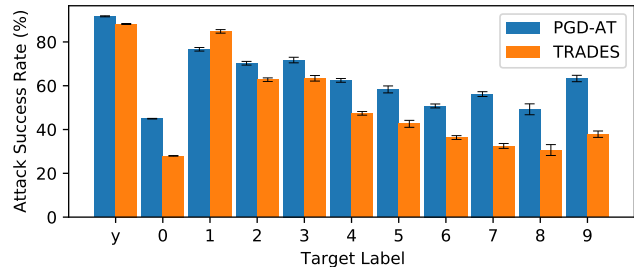
where  $x_{\text{hyp}} = \arg \min_{\|x' - x\| \leq \epsilon} \text{CE}(\mathbf{p}_\theta(x'), y)$  as in Section 3, and  $\lambda$  is the hyperparameter to control the trade-off.

Table 3: Verification accuracy (%) of adversarially trained ResNet-18 models under  $\ell_\infty$  threat model across different datasets. Standard deviations of 5 random runs are given in Appendix B Table 8.

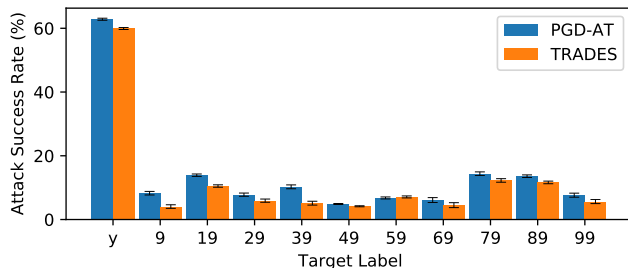
Threat Model	Model	CIFAR-10			CIFAR-100			Tiny-ImageNet		
		$\mathcal{D}$	$\mathcal{A}$	$\mathcal{F}$	$\mathcal{D}$	$\mathcal{A}$	$\mathcal{F}$	$\mathcal{D}$	$\mathcal{A}$	$\mathcal{F}$
$\ell_\infty$ ( $\epsilon = 8/255$ )	Poisoning (NT)	11.13	0.00	100.00	34.80	0.00	100.00	34.87	0.00	100.00
	Poisoning (PGD-AT)	82.65	51.34	96.20	57.32	27.85	83.20	45.14	21.69	68.96
	Poisoning (TRADES)	80.01	52.34	94.64	56.29	29.41	81.79	46.38	21.41	73.50
	Quality (NT)	94.38	0.00	100.00	76.64	0.00	100.00	64.03	0.00	100.00
	Quality (PGD-AT)	84.08	51.98	96.92	59.19	28.21	84.87	47.23	22.03	71.95
	Quality (TRADES)	81.05	53.32	95.17	57.27	30.00	82.88	47.86	22.03	75.04



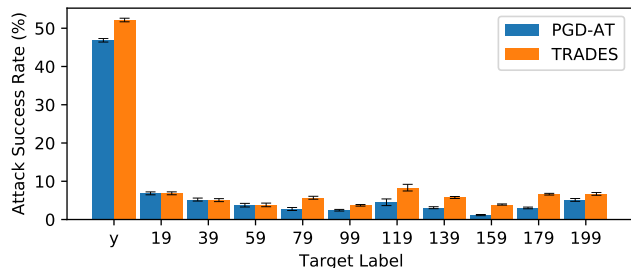
(a) CIFAR-10



(b) SVHN



(c) CIFAR-100



(d) Tiny-ImageNet

Figure 3: Attack success rate (%) of adversarially trained ResNet-18 models on misclassified examples under  $\ell_\infty$  threat model. The target label “y” denotes that the misclassified examples are perturbed to be correctly classified. The target labels “0” ~ “199” denote that the misclassified examples are perturbed to be classified as a specific target, no matter whether the target label is correct or not. Error bars indicate standard deviation over 5 random runs.

We note that Eq. (3) essentially aims to minimize a trade-off between natural risk and hypocritical risk (more details are provided in Appendix F). Thus, we term this method THRM, i.e., Trade-off for Hypocritical Risk Minimization.

Additionally, we adapt an inherently robust network architecture called  $\ell_\infty$ -dist nets (Zhang et al. 2021a) to resist hypocritical perturbations, whose technical details are deferred to Appendix G due to the space limitation.

## 5.2 Method Performance

In this subsection, we evaluate the effectiveness of the countermeasures described above. From now on, we consider the *Poisoning* and *Quality* training sets for three reasons: *i*) the *Poisoning* data can be utilized to train accurate model via adversarial training (Tao et al. 2021). *ii*) adversarial training methods are hard to fit the *Noise* and *Mislabeling* training data (Dong et al. 2021); *iii*) the *Noise* and *Mislabeling* train-

ing data can be avoided by standard data cleaning (Kandel et al. 2011), while the *Poisoning* and *Quality* data cannot, since they are correctly labelled.

**Performance of PGD-AT and TRADES.** Table 3 reports the results of PGD-AT and TRADES on CIFAR-10, CIFAR-100 and Tiny-ImageNet. We observe that the robustness of the models against hypocritical perturbations is better than the naturally trained (NT) models in Section 3.2, so is their robustness against adversarial perturbations. Nevertheless, there are still a large amount of misclassified examples that can be perturbed to be correctly classified. For example, the *Quality* (PGD-AT) model on CIFAR-10 exhibit 96.92% accuracy on hypocritically perturbed examples, while its clean accuracy is only 84.08%. Results on SVHN are deferred to Appendix B Table 9, and similar conclusions hold.

**A Closer Look at Robustness.** To directly compare the model robustness, we report the attack success rate of hyp-



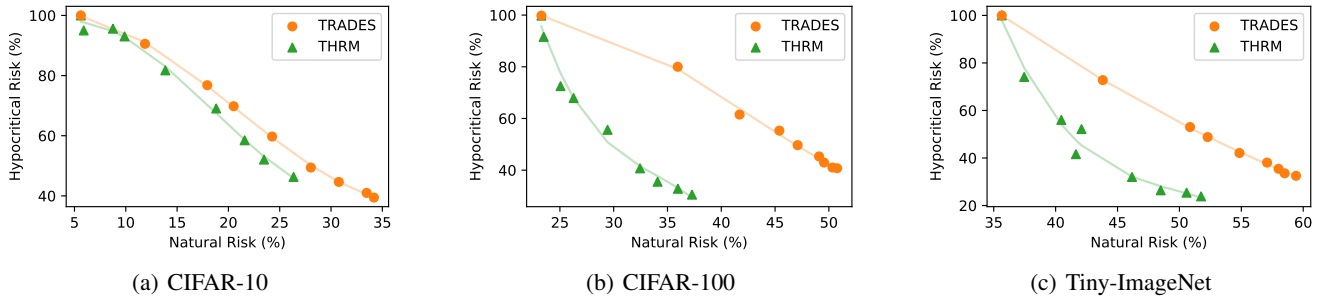


Figure 4: Empirical comparison between TRADES and THRM in terms of natural risk and the hypocritical risk on misclassified examples under  $\ell_\infty$  threat model. Each point represents a model trained on the *Quality* data with a different  $\lambda$ .

ocritical attacks (which is equivalent to the hypocritical risk on misclassified examples) for the *Quality* models in Figure 3. As a reference, we also report the success rate of targeted adversarial examples on the misclassified examples. An interesting observation is that the attack success rate of hypocritical examples is much greater than that of the targeted adversarial examples, especially on CIFAR-100 and Tiny-ImageNet, indicating that hypocritical risk may be higher than we thought. More importantly, we observe that the attack success rate of TRADES is lower than that of PGD-AT on CIFAR-10, SVHN and CIFAR-100. This indicates that TRADES is not only better than PGD-AT for adversarial robustness (which is observed in Pang et al. (2021)) but also better than PGD-AT for hypocritical robustness. One exception is that TRADES performs worse on Tiny-ImageNet. This is simply because that we set the trade-off parameter of TRADES to 6 as in (Zhang et al. 2019; Pang et al. 2021), which is too small for Tiny-ImageNet. In the next paragraph, this parameter will be tuned.

**Comparison with THRM.** We empirically compare TRADES and THRM in terms of the natural risk and the hypocritical risk on misclassified examples by tuning the regularization parameter  $\lambda$  in the range  $[0, 100]$ . The reported natural risk is estimated on clean verification data. The reported hypocritical risk is estimated on misclassified examples and is empirically approximated using PGD. Results for the models trained on the *Quality* data are summarized in Figure 4. Numerical details about the model accuracy on  $\mathcal{D}$ ,  $\mathcal{A}$ , and  $\mathcal{F}$  with different  $\lambda$  are given in Appendix B Tables 10, 11, 12, and 13. We observe that for both TRADES and THRM, as  $\lambda$  increases, the natural risk increases and the hypocritical risk decreases. It turns out that THRM achieves a better trade-off than TRADES in all cases, which is consistent with our analysis of THRM in Appendix F, and the gap between THRM and TRADES tends to increase when the number of classes is large. Therefore, when we only consider the threat of hypocritical attacks, THRM would be preferable than TRADES. However, if one wants to resist the threat of both adversarial examples and hypocritical examples, TRADES is a viable alternative.

**Results of  $\ell_\infty$ -dist nets.** Results show that  $\ell_\infty$ -dist nets achieve moderate certified hypocritical risk. For both *Quality* model and *Poisoning* model, nearly half of the errors are guaranteed not to be covered up by any attack. However,

$\ell_\infty$ -dist nets still perform worse than TRADES and THRM in terms of empirical hypocritical risk.

Overall, some improvements have been obtained, while complete robustness against hypocritical attacks still cannot be fully achieved with the current methods. Hypocritical risk remains non-negligible even after adaptive robust training. This dilemma highlights the difficulty of stabilizing models to prevent hypocritical attacks. We feel that new manners may be needed to better tackle this problem.

## 6 Conclusions and Future Directions

This paper unveils the threat of hypocritical examples in the model verification stage. Our experimental results indicate that this type of security risk is pervasive, and remains non-negligible even if adaptive countermeasures are adopted. Therefore, our investigation suggests that practitioners should be aware of this type of threat and be careful about dataset security. Below we discuss some limitations with our current study, and we also feel that our results can lead to several thought-provoking future works.

*Other performance requirements.* One may consider using adversarial perturbations to combat hypocritical attacks, i.e., estimating the robust error (Zhang et al. 2019) on the verification data. We note that this is actually equivalent to choosing the robust error as the performance requirement. It is natural then to ask whether a hypocritical attacker can cause a substandard model to exhibit high robust accuracy with small perturbations. We leave this as future work.

*Transferability.* It is also very important to study the transferability of hypocritical examples across substandard models. Transfer-based hypocritical attacks are still harmful when model structure and weights are unknown to the attacker. Understanding the transferability would help us to design effective defense strategies against the transfer-based hypocritical attacks.

*Good use of hypocritical perturbations.* We showed that many types of substandard models are susceptible to hypocritical attacks. Then, an intriguing question is whether we can turn this weakness into a strength. Specifically, one may find such a “true friend” who is capable of *consistently* helping a substandard model during the deployment stage to make correct predictions. There are concurrent works (Salman et al. 2021; Pestana et al. 2021) which explored this direction, where “robust objects” are designed to help a model to confidently detect or classify them.

## Acknowledgments

This work was supported by the National Natural Science Foundation of China (Grant No. 61732006, 62076124, and 62106028). Lei Feng was also supported by CAAI-Huawei MindSpore Open Fund.

## References

- Barocas, S.; Hardt, M.; and Narayanan, A. 2017. Fairness in machine learning. *NeurIPS Tutorial*.
- Bhatt, U.; Xiang, A.; Sharma, S.; Weller, A.; Taly, A.; Jia, Y.; Ghosh, J.; Puri, R.; Moura, J. M.; and Eckersley, P. 2020. Explainable machine learning in deployment. In *Proceedings of the 2020 Conference on Fairness, Accountability, and Transparency*.
- Biggio, B.; Corona, I.; Maiorca, D.; Nelson, B.; Šrđić, N.; Laskov, P.; Giacinto, G.; and Roli, F. 2013. Evasion attacks against machine learning at test time. In *ECML-PKDD*.
- Biggio, B.; Nelson, B.; and Laskov, P. 2012. Poisoning attacks against support vector machines. In *ICML*.
- Biggio, B.; and Roli, F. 2018. Wild patterns: Ten years after the rise of adversarial machine learning. *Pattern Recognition*.
- Blum, A.; Hanneke, S.; Qian, J.; and Shao, H. 2021. Robust learning under clean-label attack. In *COLT*.
- Bojarski, M.; Del Testa, D.; Dworakowski, D.; Firner, B.; Flepp, B.; Goyal, P.; Jackel, L. D.; Monfort, M.; Muller, U.; Zhang, J.; et al. 2016. End to end learning for self-driving cars. In *NeurIPS Deep Learning Symposium*.
- Boopathy, A.; Weng, T.-W.; Chen, P.-Y.; Liu, S.; and Daniel, L. 2019. Cnn-cert: An efficient framework for certifying robustness of convolutional neural networks. In *AAAI*.
- Buckland, M.; and Gey, F. 1994. The relationship between recall and precision. *American society for information science*.
- Carlini, N.; and Wagner, D. 2017. Towards evaluating the robustness of neural networks. In *S&P*.
- Chen, P.-Y.; Sharma, Y.; Zhang, H.; Yi, J.; and Hsieh, C.-J. 2018. Ead: elastic-net attacks to deep neural networks via adversarial examples. In *AAAI*.
- Croce, F.; and Hein, M. 2020. Reliable evaluation of adversarial robustness with an ensemble of diverse parameter-free attacks. In *ICML*.
- Cullina, D.; Bhagoji, A. N.; and Mittal, P. 2018. PAC-learning in the presence of evasion adversaries. In *NeurIPS*.
- Daniely, A.; and Schacham, H. 2020. Most ReLU Networks Suffer from  $\ell_2$  Adversarial Perturbations. In *NeurIPS*.
- Dathathri, S.; Dvijotham, K.; Kurakin, A.; Raghunathan, A.; Uesato, J.; Bunel, R.; Shankar, S.; Steinhart, J.; Goodfellow, I.; Liang, P.; et al. 2020. Enabling certification of verification-agnostic networks via memory-efficient semidefinite programming. In *NeurIPS*.
- Deng, J.; Dong, W.; Socher, R.; Li, L.-J.; Li, K.; and Fei-Fei, L. 2009. Imagenet: A large-scale hierarchical image database. In *CVPR*.
- Dong, Y.; Liao, F.; Pang, T.; Su, H.; Zhu, J.; Hu, X.; and Li, J. 2018. Boosting adversarial attacks with momentum. In *CVPR*.
- Dong, Y.; Xu, K.; Yang, X.; Pang, T.; Deng, Z.; Su, H.; and Zhu, J. 2021. Exploring Memorization in Adversarial Training. *arXiv preprint arXiv:2106.01606*.
- Elsayed, G. F.; Goodfellow, I.; and Sohl-Dickstein, J. 2019. Adversarial reprogramming of neural networks. In *ICLR*.
- Feng, J.; Cai, Q.-Z.; and Zhou, Z.-H. 2019. Learning to confuse: generating training time adversarial data with auto-encoder. In *NeurIPS*.
- Fowl, L.; Goldblum, M.; Chiang, P.-y.; Geiping, J.; Czaja, W.; and Goldstein, T. 2021. Adversarial Examples Make Strong Poisons. In *NeurIPS*.
- Gao, J.; Karbasi, A.; and Mahmoody, M. 2021. Learning and Certification under Instance-targeted Poisoning. In *UAI*.
- Geiping, J.; Fowl, L.; Somepalli, G.; Goldblum, M.; Moeller, M.; and Goldstein, T. 2021a. What Doesn't Kill You Makes You Robust (er): Adversarial Training against Poisons and Backdoors. *arXiv preprint arXiv:2102.13624*.
- Geiping, J.; Fowl, L. H.; Huang, W. R.; Czaja, W.; Taylor, G.; Moeller, M.; and Goldstein, T. 2021b. Witches' Brew: Industrial Scale Data Poisoning via Gradient Matching. In *ICLR*.
- Glorot, X.; Bordes, A.; and Bengio, Y. 2011. Deep sparse rectifier neural networks. In *AISTATS*.
- Goldblum, M.; Tsipras, D.; Xie, C.; Chen, X.; Schwarzschild, A.; Song, D.; Madry, A.; Li, B.; and Goldstein, T. 2020. Dataset Security for Machine Learning: Data Poisoning, Backdoor Attacks, and Defenses. *arXiv preprint arXiv:2012.10544*.
- Goodfellow, I. J.; Shlens, J.; and Szegedy, C. 2015. Explaining and harnessing adversarial examples. In *ICLR*.
- Gowal, S.; Dvijotham, K. D.; Stanforth, R.; Bunel, R.; Qin, C.; Uesato, J.; Arandjelovic, R.; Mann, T.; and Kohli, P. 2019. Scalable verified training for provably robust image classification. In *ICCV*.
- He, K.; Zhang, X.; Ren, S.; and Sun, J. 2015. Delving deep into rectifiers: Surpassing human-level performance on imagenet classification. In *ICCV*.
- He, K.; Zhang, X.; Ren, S.; and Sun, J. 2016. Deep residual learning for image recognition. In *CVPR*.
- Huang, H.; Ma, X.; Erfani, S. M.; Bailey, J.; and Wang, Y. 2021a. Unlearnable Examples: Making Personal Data Unexploitable. In *ICLR*.
- Huang, H.; Wang, Y.; Erfani, S. M.; Gu, Q.; Bailey, J.; and Ma, X. 2021b. Exploring Architectural Ingredients of Adversarially Robust Deep Neural Networks. In *NeurIPS*.
- Ilyas, A.; Santurkar, S.; Engstrom, L.; Tran, B.; and Madry, A. 2019. Adversarial Examples Are Not Bugs, They Are Features. In *NeurIPS*.
- Kandel, S.; Paepcke, A.; Hellerstein, J.; and Heer, J. 2011. Wrangler: Interactive visual specification of data transformation scripts. In *CHI Conference on Human Factors in Computing Systems*.
- Katz, G.; Barrett, C.; Dill, D. L.; Julian, K.; and Kochenderfer, M. J. 2017. Reluplex: An efficient SMT solver for verifying deep neural networks. In *CAV*.
- Koh, P. W.; and Liang, P. 2017. Understanding black-box predictions via influence functions. In *ICML*.
- Krizhevsky, A.; and Hinton, G. 2009. Learning multiple layers of features from tiny images. *Technical Report*.
- Kurakin, A.; Goodfellow, I.; Bengio, S.; et al. 2016. Adversarial examples in the physical world.
- Liu, Y.; Chen, X.; Liu, C.; and Song, D. 2017. Delving into transferable adversarial examples and black-box attacks. In *ICLR*.
- Madry, A.; Makelov, A.; Schmidt, L.; Tsipras, D.; and Vladu, A. 2018. Towards Deep Learning Models Resistant to Adversarial Attacks. In *ICLR*.
- Moosavi-Dezfooli, S.-M.; Fawzi, A.; and Frossard, P. 2016. DeepFool: a simple and accurate method to fool deep neural networks. In *CVPR*.



- Nakkiran, P. 2019. A Discussion of 'Adversarial Examples Are Not Bugs, They Are Features': Adversarial Examples are Just Bugs, Too. *Distill*.
- Netzer, Y.; Wang, T.; Coates, A.; Bissacco, A.; Wu, B.; and Ng, A. Y. 2011. Reading digits in natural images with unsupervised feature learning.
- Newsome, J.; Karp, B.; and Song, D. 2005. Polygraph: Automatically generating signatures for polymorphic worms. In *S&P*.
- Newsome, J.; Karp, B.; and Song, D. 2006. Paragraph: Thwarting signature learning by training maliciously. In *International Workshop on Recent Advances in Intrusion Detection*. Springer.
- Niyogi, P.; and Girosi, F. 1996. On the relationship between generalization error, hypothesis complexity, and sample complexity for radial basis functions. *Neural Computation*, 8(4): 819–842.
- Northcutt, C. G.; Athalye, A.; and Mueller, J. 2021. Pervasive Label Errors in Test Sets Destabilize Machine Learning Benchmarks. In *NeurIPS 2021 Datasets and Benchmarks Track*.
- Paley, A.; Urma, R.-G.; and Lawrence, N. D. 2020. Challenges in deploying machine learning: a survey of case studies. In *NeurIPS Workshops*.
- Pang, T.; Yang, X.; Dong, Y.; Su, H.; and Zhu, J. 2021. Bag of tricks for adversarial training. In *ICLR*.
- Pang, T.; Yang, X.; Dong, Y.; Xu, T.; Zhu, J.; and Su, H. 2020. Boosting Adversarial Training with Hypersphere Embedding. In *NeurIPS*.
- Papernot, N.; McDaniel, P.; Jha, S.; Fredrikson, M.; Celik, Z. B.; and Swami, A. 2016. The limitations of deep learning in adversarial settings. In *EuroS&P*.
- Paterson, C.; Calinescu, R.; and Ashmore, R. 2021. Assuring the Machine Learning Lifecycle: Desiderata, Methods, and Challenges. *ACM Computing Surveys*.
- Pestana, C.; Liu, W.; Glatz, D.; Owens, R.; and Mian, A. 2021. Assistive Signals for Deep Neural Network Classifiers. In *CVPR Workshops*.
- Radiya-Dixit, E.; and Tramèr, F. 2021. Data Poisoning Won't Save You From Facial Recognition. In *ICML Workshops*.
- Raghunathan, A.; Steinhardt, J.; and Liang, P. 2018. Certified defenses against adversarial examples. In *ICLR*.
- Rice, L.; Wong, E.; and Kolter, Z. 2020. Overfitting in adversarially robust deep learning. In *ICML*.
- Salman, H.; Ilyas, A.; Engstrom, L.; Vemprala, S.; Madry, A.; and Kapoor, A. 2021. Unadversarial examples: Designing objects for robust vision. In *NeurIPS*.
- Salman, H.; Yang, G.; Zhang, H.; Hsieh, C.-J.; and Zhang, P. 2019. A Convex Relaxation Barrier to Tight Robustness Verification of Neural Networks. In *NeurIPS*.
- Sambasivan, N.; Kapania, S.; Highfill, H.; Akrong, D.; Paritosh, P. K.; and Aroyo, L. M. 2021. "Everyone wants to do the model work, not the data work": Data Cascades in High-Stakes AI. In *CHI Conference on Human Factors in Computing Systems*.
- Shafahi, A.; Huang, W. R.; Najibi, M.; Suci, O.; Studer, C.; Dumitras, T.; and Goldstein, T. 2018. Poison frogs! targeted clean-label poisoning attacks on neural networks. In *NeurIPS*.
- Shi, Z.; Wang, Y.; Zhang, H.; Yi, J.; and Hsieh, C.-J. 2021. Fast Certified Robust Training with Short Warmup. In *NeurIPS*.
- Simonyan, K.; and Zisserman, A. 2015. Very deep convolutional networks for large-scale image recognition. In *ICLR*.
- Szegedy, C.; Zaremba, W.; Sutskever, I.; Bruna, J.; Erhan, D.; Goodfellow, I.; and Fergus, R. 2014. Intriguing properties of neural networks. In *ICLR*.
- Tao, L.; Feng, L.; Yi, J.; Huang, S.-J.; and Chen, S. 2021. Better Safe Than Sorry: Preventing Delusively Adversaries with Adversarial Training. In *NeurIPS*.
- Tsipras, D.; Santurkar, S.; Engstrom, L.; Turner, A.; and Madry, A. 2019. Robustness may be at odds with accuracy. In *ICLR*.
- Uesato, J.; O'donoghue, B.; Kohli, P.; and Oord, A. 2018. Adversarial risk and the dangers of evaluating against weak attacks. In *ICML*.
- Wang, L.; Zhang, H.; Yi, J.; Hsieh, C.-J.; and Jiang, Y. 2020a. Spanning attack: reinforce black-box attacks with unlabeled data. *Machine Learning*.
- Wang, Y.; Zou, D.; Yi, J.; Bailey, J.; Ma, X.; and Gu, Q. 2020b. Improving adversarial robustness requires revisiting misclassified examples. In *ICLR*.
- Weng, L.; Zhang, H.; Chen, H.; Song, Z.; Hsieh, C.-J.; Daniel, L.; Boning, D.; and Dhillon, I. 2018. Towards fast computation of certified robustness for relu networks. In *ICML*.
- Wong, E.; and Kolter, Z. 2018. Provable defenses against adversarial examples via the convex outer adversarial polytope. In *ICML*.
- Wu, D.; Xia, S.-T.; and Wang, Y. 2020. Adversarial weight perturbation helps robust generalization. In *NeurIPS*.
- Xu, K.; Zhang, H.; Wang, S.; Wang, Y.; Jana, S.; Lin, X.; and Hsieh, C.-J. 2021. Fast and Complete: Enabling Complete Neural Network Verification with Rapid and Massively Parallel Incomplete Verifiers. In *ICLR*.
- Yao, L.; and Miller, J. 2015. Tiny imagenet classification with convolutional neural networks. *CS 231N*, 2(5): 8.
- Zagoruyko, S.; and Komodakis, N. 2016. Wide residual networks. *arXiv preprint arXiv:1605.07146*.
- Zhai, R.; Dan, C.; He, D.; Zhang, H.; Gong, B.; Ravikumar, P.; Hsieh, C.-J.; and Wang, L. 2020. Macer: Attack-free and scalable robust training via maximizing certified radius. In *ICLR*.
- Zhang, B.; Cai, T.; Lu, Z.; He, D.; and Wang, L. 2021a. Towards Certifying L-infinity Robustness using Neural Networks with L-inf-dist Neurons. In *ICML*.
- Zhang, C.; Bengio, S.; Hardt, M.; Recht, B.; and Vinyals, O. 2017. Understanding deep learning requires rethinking generalization. In *ICLR*.
- Zhang, H.; Chen, H.; Xiao, C.; Gowal, S.; Stanforth, R.; Li, B.; Boning, D.; and Hsieh, C.-J. 2020a. Towards Stable and Efficient Training of Verifiably Robust Neural Networks. In *ICLR*.
- Zhang, H.; Weng, T.-W.; Chen, P.-Y.; Hsieh, C.-J.; and Daniel, L. 2018. Efficient Neural Network Robustness Certification with General Activation Functions. In *NeurIPS*.
- Zhang, H.; Yu, Y.; Jiao, J.; King, E.; El Ghaoui, L.; and Jordan, M. 2019. Theoretically principled trade-off between robustness and accuracy. In *ICML*.
- Zhang, J.; Xu, X.; Han, B.; Niu, G.; Cui, L.; Sugiyama, M.; and Kankanhalli, M. 2020b. Attacks which do not kill training make adversarial learning stronger. In *ICML*.
- Zhang, J.; Zhu, J.; Niu, G.; Han, B.; Sugiyama, M.; and Kankanhalli, M. 2021b. Geometry-aware instance-reweighted adversarial training. In *ICLR*.
- Zheng, S.; Song, Y.; Leung, T.; and Goodfellow, I. 2016. Improving the robustness of deep neural networks via stability training. In *CVPR*.
- Zhu, C.; Huang, W. R.; Li, H.; Taylor, G.; Studer, C.; and Goldstein, T. 2019. Transferable Clean-Label Poisoning Attacks on Deep Neural Nets. In *ICML*.

## A Experimental Setup

To reveal the worst-case risk, our experiments focus on white-box attacks. Therefore, the hypocritical examples in Section 3 and Section 5 are carefully crafted for each model after training. We also note that it is possible for future research to compute hypocritical examples before training via transfer-based attacks. Our experiments run with NVIDIA GeForce RTX 2080 Ti GPUs. Our implementation is based on PyTorch, and the code to reproduce our results available at <https://github.com/TLMichael/False-Friends>.

### A.1 Datasets

**CIFAR-10<sup>4</sup>**. This dataset (Krizhevsky and Hinton 2009) consists of 60,000  $32 \times 32$  colour images (50,000 images for training and 10,000 images for evaluation) in 10 classes (“airplane”, “car”, “bird”, “cat”, “deer”, “dog”, “frog”, “horse”, “ship”, and “truck”). We use the original test set as the clean verification data. We adopt various architectures for this dataset, including MLP, VGG-16 (Simonyan and Zisserman 2015), ResNet-18 (He et al. 2016), and WideResNet-28-10 (Zagoruyko and Komodakis 2016). A four-layer MLP (2 hidden layers, 3072 neurons in each) with ReLU activations (Glorot, Bordes, and Bengio 2011) is used here. The models are initialized with the commonly used He initialization (He et al. 2015), which is the default initialization in torchvision<sup>5</sup>. The initial learning rate is set to 0.1, except for MLP and VGG-16 on Noise and Mislabeling, where the initial learning rate is set to 0.01. Following Pang et al. (2021), in the default setting, the models are trained for 110 epochs using SGD with momentum 0.9, batch size 128, and weight decay  $5 \times 10^{-4}$ , where the learning rate is decayed by a factor of 0.1 in the 100th and 105th epochs, and simple data augmentations such as  $32 \times 32$  random crop with 4-pixel padding and random horizontal flip are applied. Following Zhang et al. (2017), when training on the *Noise* and *Mislabeling* data, data augmentations and weight decay are turned off<sup>6</sup>.

**SVHN<sup>7</sup>**. This dataset (Netzer et al. 2011) consists of 630,420  $32 \times 32$  colour images (73,257 images for training and 26,032 images for evaluation) in 10 classes. We use the original test set as the clean verification data. We adopt the ResNet-18 architecture for this dataset. The model is initialized with the commonly used He initialization. The initial learning rate is set to 0.01. In the default setting, the models are trained for 60 epochs using SGD with momentum 0.9, batch size 128, and weight decay  $5 \times 10^{-4}$ , where the learning rate is decayed by a factor of 0.1 in the 50th and 55th epochs, and simple data augmentation such as  $32 \times 32$  random crop with 4-pixel padding is applied. when training on the *Noise* and *Mislabeling* data, data augmentation and weight decay are turned off.

**CIFAR-100<sup>8</sup>**. This dataset (Krizhevsky and Hinton 2009) consists of 60,000  $32 \times 32$  colour images (50,000 images for training and 10,000 images for evaluation) in 100 classes. We use the original test set as the clean verification data. We adopt the ResNet-18 architecture for this dataset. The model is initialized with the commonly used He initialization. The initial learning rate is set to 0.1. In the default setting, the models are trained for 110 epochs using SGD with momentum 0.9, batch size 128, and weight decay  $5 \times 10^{-4}$ , where the learning rate is decayed by a factor of 0.1 in the 100th and 105th epochs, and simple data augmentations such as  $32 \times 32$  random crop with 4-pixel padding and random horizontal flip are applied. when training on the *Noise* and *Mislabeling* data, data augmentations and weight decay are turned off.

**Tiny-ImageNet<sup>9</sup>**. This dataset (Yao and Miller 2015) consists of 110000  $64 \times 64$  colour images (100,000 images for training and 10,000 images for evaluation) in 200 classes. We use the original validation set as the clean verification data. We adopt the ResNet-18 architecture for this dataset. The model is initialized with the commonly used He initialization. The initial learning rate is set to 0.1. In the default setting, the models are trained for 60 epochs using SGD with momentum 0.9, batch size 64, and weight decay  $5 \times 10^{-4}$ , where the learning rate is decayed by a factor of 0.1 in the 50th and 55th epochs, and simple data augmentations such as  $64 \times 64$  random crop with 4-pixel padding and random horizontal flip are applied. when training on the *Noise* and *Mislabeling* data, data augmentation and weight decay are turned off.

### A.2 Robust Training

We perform robust training algorithms including PGD-AT, TRADES, and THRM by following the common settings (Madry et al. 2018; Pang et al. 2021). Specifically, we train against a projected gradient descent (PGD) attacker, starting from a random initial perturbation of the training data. We use 10/20 steps of PGD with a step size of  $\epsilon/4$  for training/evaluation. We consider adversarial perturbations in  $\ell_p$  norm where  $p = \{2, \infty\}$ . For  $\ell_2$  threat model,  $\epsilon = 0.5$ . For  $\ell_\infty$  threat model,  $\epsilon = 8/255$ .

<sup>4</sup><https://www.cs.toronto.edu/~kriz/cifar.html>

<sup>5</sup><https://github.com/pytorch/vision/tree/master/torchvision/models>

<sup>6</sup><https://github.com/pluskid/fitting-random-labels>

<sup>7</sup><http://ufldl.stanford.edu/housenumbers/>

<sup>8</sup><https://www.cs.toronto.edu/~kriz/cifar.html>

<sup>9</sup><http://cs231n.stanford.edu/tiny-imagenet-200.zip>

### A.3 Low-Quality Training Data

The *Noisy* data is constructed by replacing the each image in the training set with uniform noise and keeping the labels unchanged (Zhang et al. 2017). The *Mislabeling* data is constructed by replacing the labels with random ones and keeping the labels unchanged (Zhang et al. 2017). The *Poisoning* data is constructed by perturbing the images to maximize generalization error and keeping the labels unchanged (Ilyas et al. 2019; Nakkiran 2019). Following Tao et al. (2021), each input-label pair  $(\mathbf{x}, y)$  in the *Poisoning* data is constructed as follows. We first select a target class  $t$  deterministically according to the source class  $y$  (e.g., using a fixed permutation of labels). Then, we add a small adversarial perturbation to  $\mathbf{x}$  to ensure that it is misclassified as  $t$  by a naturally trained model, that is,  $\mathbf{x}_{\text{adv}} = \arg \min_{\|\mathbf{x}' - \mathbf{x}\| \leq \epsilon} \text{CE}(f(\mathbf{x}'), t)$ . Here  $f$  is a naturally trained model on the *Quality* data. Finally, we assign the correct label  $y$  to the perturbed input. The resulting input-label pairs  $(\mathbf{x}_{\text{adv}}, y)$  make up the *Poisoning* dataset. Perturbations are constrained in  $\ell_2$ -norm with  $\epsilon = 0.5$  or  $\ell_\infty$ -norm with  $\epsilon = 8/255$ . The number of PGD iterations is set to 100 and step size is set to  $\epsilon/5$ .

## B Omitted Tables and Figures

Table 4: Verification examples for the naturally trained models. These examples are originally misclassified (as red labels) by the models, but they are correctly classified (as green labels) after adding hypocritical perturbations. Perturbations are rescaled for display.






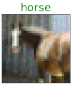



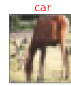

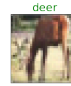





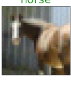



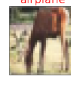

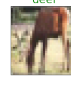

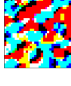

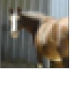

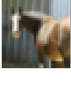
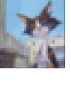
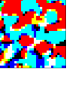
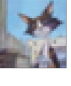
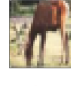

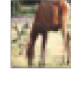
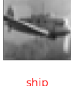

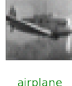
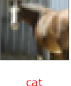

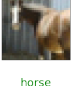
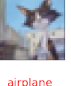

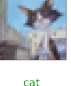
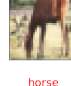

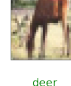



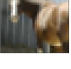

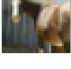
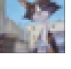

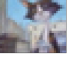
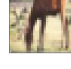

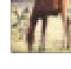
Model	Example #422			Example #4503			Example #8778			Example #9910		
Naive												
Noise												
Mislabeling												
Poisoning												
Quality												

Table 5: Verification accuracy (%) of substandard models on CIFAR-10 under  $\ell_\infty$  threat model across different architectures.  $\mathcal{D}$ ,  $\mathcal{A}$ , and  $\mathcal{F}$  denote the model accuracy evaluated on clean examples, adversarially perturbed examples, and hypocritically perturbed examples, respectively. We report mean and standard deviation over 5 random runs.

Model	MLP			VGG-16			WideResNet-28-10		
	$\mathcal{D}$	$\mathcal{A}$	$\mathcal{F}$	$\mathcal{D}$	$\mathcal{A}$	$\mathcal{F}$	$\mathcal{D}$	$\mathcal{A}$	$\mathcal{F}$
Naive	8.56±1.20	0.00±0.00	99.56±0.50	9.76±0.34	0.45±0.99	57.25±26.53	10.06±0.14	0.34±0.65	40.64±14.66
Noise	8.53±0.77	0.71±0.46	86.75±0.34	9.81±1.17	0.00±0.01	97.98±3.60	11.35±1.22	0.02±0.05	98.42±1.66
Mislabeling	9.92±0.18	0.00±0.00	100.00±0.00	9.94±0.20	0.00±0.00	99.86±0.10	10.21±0.17	0.00±0.00	100.00±0.00
Poisoning	57.60±0.17	0.55±0.05	99.50±0.05	12.19±0.88	0.00±0.00	99.49±0.17	10.42±1.16	0.00±0.00	100.00±0.00
Quality	58.09±0.21	0.91±0.07	99.31±0.07	92.90±0.08	0.00±0.00	100.00±0.00	95.41±0.13	0.00±0.00	100.00±0.00

Table 6: Verification accuracy (%) of substandard models on CIFAR-10 under  $\ell_2$  threat model across different architectures.  $\mathcal{D}$ ,  $\mathcal{A}$ , and  $\mathcal{F}$  denote the model accuracy evaluated on clean examples, adversarially perturbed examples, and hypocritically perturbed examples, respectively. We report mean and standard deviation over 5 random runs.

Model	MLP			VGG-16			WideResNet-28-10		
	$\mathcal{D}$	$\mathcal{A}$	$\mathcal{F}$	$\mathcal{D}$	$\mathcal{A}$	$\mathcal{F}$	$\mathcal{D}$	$\mathcal{A}$	$\mathcal{F}$
Naive	8.56±1.20	0.07±0.05	72.75±2.79	9.76±0.34	3.28±4.22	33.24±23.10	10.06±0.14	4.85±3.95	19.52±8.43
Noise	8.53±0.77	0.79±0.45	74.32±2.44	11.13±1.32	0.00±0.00	76.63±12.49	9.07±1.56	0.34±0.36	81.83±10.68
Mislabeling	9.92±0.18	0.00±0.00	97.75±0.08	10.00±0.46	0.01±0.01	89.71±1.20	10.07±0.14	0.00±0.00	99.99±0.01
Poisoning	57.97±0.28	19.70±0.43	88.52±0.25	23.61±1.45	0.00±0.00	99.85±0.13	18.57±1.35	0.00±0.00	100.00±0.00
Quality	58.09±0.21	19.76±0.51	88.74±0.20	92.99±0.14	0.21±0.06	100.00±0.00	95.44±0.09	0.03±0.01	100.00±0.00

Table 7: Verification accuracy (%) of substandard ResNet-18 models under  $\ell_\infty$  threat model across different datasets.  $\mathcal{D}$ ,  $\mathcal{A}$ , and  $\mathcal{F}$  denote the model accuracy evaluated on clean examples, adversarially perturbed examples, and hypocritically perturbed examples, respectively. We report mean and standard deviation over 5 random runs.

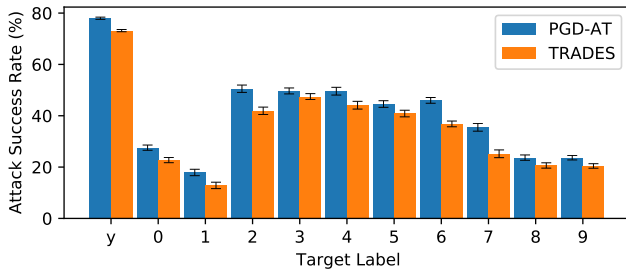
Model	SVHN			CIFAR-100			Tiny-ImageNet		
	$\mathcal{D}$	$\mathcal{A}$	$\mathcal{F}$	$\mathcal{D}$	$\mathcal{A}$	$\mathcal{F}$	$\mathcal{D}$	$\mathcal{A}$	$\mathcal{F}$
Naive	10.73±4.30	0.85±1.89	55.64±23.16	0.98±0.09	0.02±0.05	7.26±3.12	0.49±0.05	0.04±0.08	4.50±3.17
Noise	10.76±2.04	0.00±0.00	99.96±0.09	1.02±0.14	0.01±0.01	81.93±23.14	0.39±0.05	0.01±0.01	74.58±27.88
Mislabeling	9.77±0.16	0.00±0.00	100.00±0.00	0.99±0.08	0.00±0.00	99.81±0.10	0.48±0.08	0.00±0.00	99.99±0.01
Poisoning	41.42±0.73	0.00±0.00	100.00±0.00	34.80±0.56	0.00±0.00	100.00±0.00	34.87±0.27	0.00±0.00	100.00±0.00
Quality	96.57±0.14	0.32±0.05	99.99±0.00	76.64±0.18	0.01±0.00	99.96±0.03	64.03±0.14	0.02±0.02	100.00±0.00

Table 8: Verification accuracy (%) of adversarially trained ResNet-18 models under  $\ell_\infty$  threat model across different datasets.  $\mathcal{D}$ ,  $\mathcal{A}$ , and  $\mathcal{F}$  denote the model accuracy evaluated on clean examples, adversarially perturbed examples, and hypocritically perturbed examples, respectively. We report mean and standard deviation over 5 random runs.

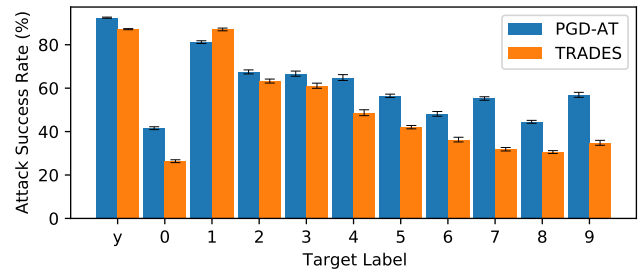
Model	CIFAR-10			CIFAR-100			Tiny-ImageNet		
	$\mathcal{D}$	$\mathcal{A}$	$\mathcal{F}$	$\mathcal{D}$	$\mathcal{A}$	$\mathcal{F}$	$\mathcal{D}$	$\mathcal{A}$	$\mathcal{F}$
Poisoning (PGD-AT)	82.65±0.14	51.34±0.23	96.2±0.07	57.32±0.16	27.85±0.13	83.2±0.14	45.14±0.25	21.69±0.11	68.96±0.29
Poisoning (TRADES)	80.01±0.17	52.34±0.18	94.64±0.08	56.29±0.33	29.41±0.25	81.79±0.17	46.38±0.20	21.41±0.10	73.5±0.21
Quality (PGD-AT)	84.08±0.18	51.98±0.24	96.92±0.09	59.19±0.27	28.21±0.16	84.87±0.10	47.23±0.22	22.03±0.17	71.95±0.22
Quality (TRADES)	81.05±0.14	53.32±0.21	95.17±0.18	57.27±0.04	30.00±0.30	82.88±0.32	47.86±0.09	22.03±0.16	75.04±0.18

Table 9: Verification accuracy (%) of adversarially trained ResNet-18 models on SVHN under  $\ell_\infty$  threat model.  $\mathcal{D}$ ,  $\mathcal{A}$ , and  $\mathcal{F}$  denote the model accuracy evaluated on clean examples, adversarially perturbed examples, and hypocritically perturbed examples, respectively. We report mean and standard deviation over 5 random runs.

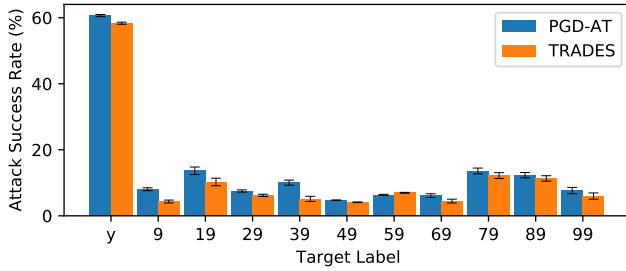
Model	SVHN		
	$\mathcal{D}$	$\mathcal{A}$	$\mathcal{F}$
Poisoning (PGD-AT)	90.50±0.14	54.17±0.16	99.28±0.02
Poisoning (TRADES)	87.34±0.40	54.92±0.15	98.38±0.10
Quality (PGD-AT)	93.37±1.49	56.29±2.21	99.45±0.13
Quality (TRADES)	90.69±0.30	59.78±0.31	98.90±0.07



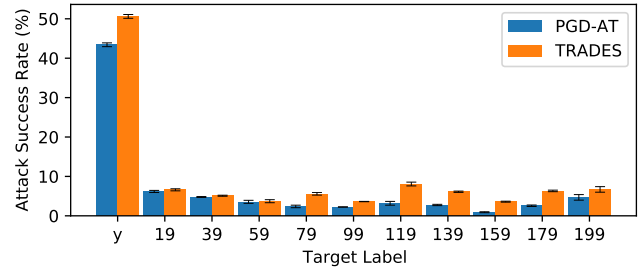
(a) CIFAR-10



(b) SVHN



(c) CIFAR-100



(d) Tiny-ImageNet

Figure 5: Attack success rate (%) of adversarially trained ResNet-18 models on misclassified examples under  $\ell_\infty$  threat model. Here, the models are trained on the *Poisoning* data, and conclusions similar to Figure 3 in the main text similarly hold. The target label “y” denotes that the misclassified examples are perturbed to be correctly classified. The target labels “0” ~ “199” denote that the misclassified examples are perturbed to be classified as a specific target, no matter whether the target label is correct or not. Error bars indicate standard deviation over 5 random runs.

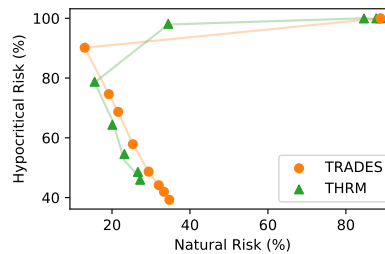


Figure 6: Empirical comparison between TRADES and THRM in terms of the natural risk and the hypocritical risk on misclassified examples under  $\ell_\infty$  threat model. Each point represents a model with a different  $\lambda$ . Here, the models are trained on the *Poisoning* data of CIFAR-10. We observe that, when  $\lambda$  is small, TRADES is better than THRM. This is because TRADES can defense against the Poisoning data (Nakkiran 2019) by minimizing the adversarial risk (Tao et al. 2021), while THRM cannot. However, we note that, when  $\lambda$  is large, THRM can achieve a better trade-off than TRADES. This may be due to that training model using THRM with large  $\lambda$  can somewhat bring nontrivial robustness to adversarial perturbations, as shown in Table 13 and Figure 7.

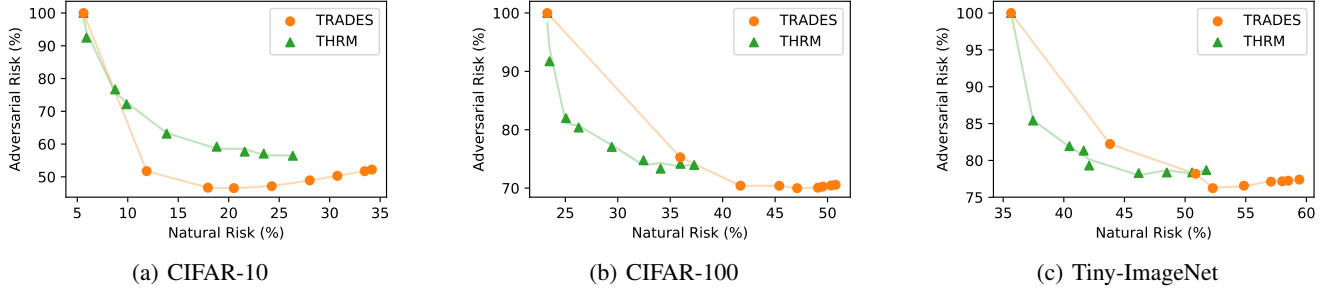


Figure 7: Empirical comparison between TRADES and THRM in terms of natural risk and the adversarial risk on all examples under  $\ell_\infty$  threat model. Each point represents a model trained on the *Quality* data with a different  $\lambda$ . **Description:** This is a plot to illustrate adversarial risk. The results show that *THRM achieves considerable adversarial robustness* compared with TRADES. We note that THRM is only designed to minimize natural and hypocritical risks. Thus, it is intriguing in some sense that it can achieve considerable adversarial risk. A possible explanation for this might be that improving the hypocritical risk somehow decreases the Lipschitz constant of the model, thereby reducing the adversarial risk.

Table 10: Empirical comparison between TRADES and THRM on CIFAR-10 under  $\ell_\infty$  threat model. The models are trained on the *Quality* data.

Method	$\lambda$	Accuracy			Risk		
		$\mathcal{D}$	$\mathcal{A}$	$\mathcal{F}$	$\mathcal{R}_{\text{nat}}(f, \mathcal{D})$	$\mathcal{R}_{\text{adv}}(f, \mathcal{D}_f^+)$	$\mathcal{R}_{\text{hyp}}(f, \mathcal{D}_f^-)$
THRM	0	94.38	0.00	100.00	5.62	100.00	100.00
	1	94.10	7.53	99.70	5.90	92.00	94.92
	5	91.25	23.32	99.65	8.75	74.44	96.00
	10	90.12	27.83	99.31	9.88	69.12	93.02
	20	86.15	36.82	97.47	13.85	57.26	81.73
	40	81.19	40.80	94.18	18.81	49.75	69.06
	60	78.42	42.30	91.04	21.58	46.06	58.48
	80	76.53	42.91	88.75	23.47	43.93	52.07
	100	73.65	43.56	85.85	26.35	40.86	46.30
	TRADES	0	94.38	0.00	100.00	5.62	100.00
1		88.13	48.26	98.88	11.87	45.24	90.56
5		82.06	53.30	95.84	17.94	35.05	76.81
10		79.49	53.44	93.81	20.51	32.77	69.82
20		75.74	52.84	90.23	24.26	30.24	59.73
40		71.97	51.08	85.82	28.03	29.03	49.41
60		69.24	49.70	82.97	30.76	28.22	44.64
80		66.53	48.27	80.25	33.47	27.45	40.99
100		65.82	47.78	79.30	34.18	27.41	39.44



Table 11: Empirical comparison between TRADES and THRM on CIFAR-100 under  $\ell_\infty$  threat model. The models are trained on the *Quality* data.

Method	$\lambda$	Accuracy			Risk		
		$\mathcal{D}$	$\mathcal{A}$	$\mathcal{F}$	$\mathcal{R}_{\text{nat}}(f, \mathcal{D})$	$\mathcal{R}_{\text{adv}}(f, \mathcal{D}_f^+)$	$\mathcal{R}_{\text{hyp}}(f, \mathcal{D}_f^-)$
THRM	0	76.72	0.01	99.95	23.28	99.99	99.79
	1	76.51	8.28	98.02	23.49	89.18	91.57
	5	74.94	18.00	93.11	25.06	75.98	72.51
	10	73.73	19.62	91.57	26.27	73.39	67.91
	20	70.57	22.94	86.94	29.43	67.49	55.62
	40	67.55	25.21	80.76	32.45	62.68	40.71
	60	65.92	26.67	78.03	34.08	59.54	35.53
	80	64.03	25.84	75.83	35.97	59.64	32.81
	100	62.72	26.03	74.10	37.28	58.50	30.53
TRADES	0	76.72	0.01	99.95	23.28	99.99	99.79
	1	64.05	24.72	92.81	35.95	61.41	80.00
	5	58.30	29.59	83.95	41.70	49.25	61.51
	10	54.60	29.61	79.71	45.40	45.77	55.31
	20	52.90	30.01	76.30	47.10	43.27	49.68
	40	50.91	29.92	73.16	49.09	41.23	45.32
	60	50.45	29.74	71.73	49.55	41.05	42.95
	80	49.67	29.55	70.32	50.33	40.51	41.03
	100	49.23	29.43	69.92	50.77	40.22	40.75

Table 12: Empirical comparison between TRADES and THRM on Tiny-ImageNet under  $\ell_\infty$  threat model. The models are trained on the *Quality* data.

Method	$\lambda$	Accuracy			Risk		
		$\mathcal{D}$	$\mathcal{A}$	$\mathcal{F}$	$\mathcal{R}_{\text{nat}}(f, \mathcal{D})$	$\mathcal{R}_{\text{adv}}(f, \mathcal{D}_f^+)$	$\mathcal{R}_{\text{hyp}}(f, \mathcal{D}_f^-)$
THRM	0	64.35	0.00	100.00	35.65	100.00	100.00
	1	62.54	14.59	90.30	37.46	76.67	74.11
	5	57.91	18.06	79.87	42.09	68.81	52.17
	10	59.54	18.67	82.21	40.46	68.64	56.03
	20	58.36	20.69	75.69	41.64	64.55	41.62
	40	53.83	21.71	68.61	46.17	59.67	32.01
	60	51.51	21.63	64.31	48.49	58.01	26.40
	80	49.42	21.62	62.27	50.58	56.25	25.41
	100	48.25	21.31	60.60	51.75	55.83	23.86
TRADES	0	64.35	0.00	100.00	35.65	100.00	100.00
	1	56.19	17.77	88.07	43.81	68.38	72.77
	5	49.14	21.80	76.11	50.86	55.64	53.03
	10	47.72	23.76	73.24	52.28	50.21	48.81
	20	45.15	23.43	68.25	54.85	48.11	42.11
	40	42.92	22.88	64.65	57.08	46.69	38.07
	60	41.99	22.83	62.56	58.01	45.63	35.46
	80	41.50	22.75	61.14	58.50	45.18	33.57
	100	40.58	22.60	59.90	59.42	44.31	32.51

Table 13: Empirical comparison between TRADES and THRM on CIFAR-10 under  $\ell_\infty$  threat model. The models are trained on the *Poisoning* data.

Method	$\lambda$	Accuracy			Risk		
		$\mathcal{D}$	$\mathcal{A}$	$\mathcal{F}$	$\mathcal{R}_{\text{nat}}(f, \mathcal{D})$	$\mathcal{R}_{\text{adv}}(f, \mathcal{D}_f^+)$	$\mathcal{R}_{\text{hyp}}(f, \mathcal{D}_f^-)$
THRM	0	11.13	0.00	100.00	88.87	100.00	100.00
	1	12.20	0.00	99.97	87.80	100.00	99.97
	5	15.35	0.00	99.95	84.65	100.00	99.94
	10	65.57	19.45	99.36	34.43	70.34	98.14
	20	84.46	39.34	96.70	15.54	53.42	78.76
	40	79.91	43.00	92.84	20.09	46.19	64.36
	60	76.82	44.27	89.47	23.18	42.37	54.57
	80	73.35	44.67	86.30	26.65	39.10	48.59
	100	72.78	44.51	85.29	27.22	38.84	45.96
TRADES	0	11.13	0.00	100.00	88.87	100.00	100.00
	1	87.00	47.52	98.72	13.00	45.38	90.15
	5	80.81	52.17	95.13	19.19	35.44	74.62
	10	78.41	52.83	93.24	21.59	32.62	68.69
	20	74.65	51.93	89.32	25.35	30.44	57.87
	40	70.60	50.00	84.91	29.40	29.18	48.67
	60	68.01	48.92	82.13	31.99	28.07	44.14
	80	66.67	48.39	80.65	33.33	27.42	41.94
	100	65.29	47.25	78.91	34.71	27.63	39.24

## C Proofs

In this section, we provide the proofs of our theoretical results in Section 4 and Appendix G.

### C.1 Proof of Theorem 4.3

**Theorem 4.3 (restated).**  $\mathcal{R}_{\text{adv}}(f_\theta, \mathcal{D}) = \mathcal{R}_{\text{nat}}(f_\theta, \mathcal{D}) + (1 - \mathcal{R}_{\text{nat}}(f_\theta, \mathcal{D})) \cdot \mathcal{R}_{\text{adv}}(f_\theta, \mathcal{D}_f^+)$ .

*Proof.* For the sake of brevity, here we use the notation  $f$  to represent  $f_\theta$ . Denote by  $\mathbf{x}_{\text{adv}} = \arg \max_{\|\mathbf{x}' - \mathbf{x}\| \leq \epsilon} \mathbb{1}(f_\theta(\mathbf{x}') \neq y)$ , we have

$$\begin{aligned}
\mathcal{R}_{\text{adv}}(f, \mathcal{D}) &= \mathbb{E}_{(\mathbf{x}, y) \sim \mathcal{D}} \left[ \max_{\|\mathbf{x}' - \mathbf{x}\| \leq \epsilon} \mathbb{1}(f(\mathbf{x}') \neq y) \right] \\
&= \mathbb{E}_{(\mathbf{x}, y) \sim \mathcal{D}} [\mathbb{1}(f(\mathbf{x}_{\text{adv}}) \neq y)] \\
&= \mathbb{E}_{(\mathbf{x}, y) \sim \mathcal{D}} [\mathbb{1}(f(\mathbf{x}_{\text{adv}}) \neq y) \cdot 1] \\
&= \mathbb{E}_{(\mathbf{x}, y) \sim \mathcal{D}} [\mathbb{1}(f(\mathbf{x}_{\text{adv}}) \neq y) \cdot (\mathbb{1}(f(\mathbf{x}) = y) + \mathbb{1}(f(\mathbf{x}) \neq y))] \\
&= \mathbb{E}_{(\mathbf{x}, y) \sim \mathcal{D}} [\mathbb{1}(f(\mathbf{x}_{\text{adv}}) \neq y) \cdot \mathbb{1}(f(\mathbf{x}) = y)] + \mathbb{E}_{(\mathbf{x}, y) \sim \mathcal{D}} [\mathbb{1}(f(\mathbf{x}_{\text{adv}}) \neq y) \cdot \mathbb{1}(f(\mathbf{x}) \neq y)] \\
&= \mathbb{E}_{(\mathbf{x}, y) \sim \mathcal{D}} [\mathbb{1}(f(\mathbf{x}_{\text{adv}}) \neq y) \cdot \mathbb{1}(f(\mathbf{x}) = y)] + \mathbb{E}_{(\mathbf{x}, y) \sim \mathcal{D}} [\mathbb{1}(f(\mathbf{x}) \neq y)] \\
&= \mathbb{E}_{(\mathbf{x}, y) \sim \mathcal{D}} [\mathbb{1}(f(\mathbf{x}) = y)] \cdot \mathbb{E}_{(\mathbf{x}, y) \sim \mathcal{D}_f^+} [\mathbb{1}(f(\mathbf{x}_{\text{adv}}) \neq y)] + \mathbb{E}_{(\mathbf{x}, y) \sim \mathcal{D}} [\mathbb{1}(f(\mathbf{x}) \neq y)] \\
&= \mathbb{E}_{(\mathbf{x}, y) \sim \mathcal{D}} [1 - \mathbb{1}(f(\mathbf{x}) \neq y)] \cdot \mathbb{E}_{(\mathbf{x}, y) \sim \mathcal{D}_f^+} [\mathbb{1}(f(\mathbf{x}_{\text{adv}}) \neq y)] + \mathbb{E}_{(\mathbf{x}, y) \sim \mathcal{D}} [\mathbb{1}(f(\mathbf{x}) \neq y)] \\
&= (1 - \mathcal{R}_{\text{nat}}(f, \mathcal{D})) \cdot \mathcal{R}_{\text{adv}}(f, \mathcal{D}_f^+) + \mathcal{R}_{\text{nat}}(f, \mathcal{D}) \\
&= \mathcal{R}_{\text{nat}}(f, \mathcal{D}) + (1 - \mathcal{R}_{\text{nat}}(f, \mathcal{D})) \cdot \mathcal{R}_{\text{adv}}(f, \mathcal{D}_f^+)
\end{aligned}$$

□

### C.2 Proof of Theorem 4.4

**Theorem 4.4 (restated).**  $\mathcal{R}_{\text{hyp}}(f_\theta, \mathcal{D}) = 1 - (1 - \mathcal{R}_{\text{hyp}}(f_\theta, \mathcal{D}_f^-)) \cdot \mathcal{R}_{\text{nat}}(f_\theta, \mathcal{D})$ .

*Proof.* For the sake of brevity, here we use the notation  $f$  to represent  $f_\theta$ . Denote by  $\mathbf{x}_{\text{hyp}} = \arg \max_{\|\mathbf{x}' - \mathbf{x}\| \leq \epsilon} \mathbb{1}(f(\mathbf{x}') = y)$ , we have

$$\begin{aligned}
\mathcal{R}_{\text{hyp}}(f, \mathcal{D}) &= \mathbb{E}_{(\mathbf{x}, y) \sim \mathcal{D}} \left[ \max_{\|\mathbf{x}' - \mathbf{x}\| \leq \epsilon} \mathbb{1}(f(\mathbf{x}') = y) \right] \\
&= \mathbb{E}_{(\mathbf{x}, y) \sim \mathcal{D}} [\mathbb{1}(f(\mathbf{x}_{\text{hyp}}) = y)] \\
&= 1 - \mathbb{E}_{(\mathbf{x}, y) \sim \mathcal{D}} [\mathbb{1}(f(\mathbf{x}_{\text{hyp}}) \neq y)] \\
&= 1 - \mathbb{E}_{(\mathbf{x}, y) \sim \mathcal{D}} [\mathbb{1}(f(\mathbf{x}_{\text{hyp}}) \neq y) \cdot 1] \\
&= 1 - \mathbb{E}_{(\mathbf{x}, y) \sim \mathcal{D}} [\mathbb{1}(f(\mathbf{x}_{\text{hyp}}) \neq y) \cdot (\mathbb{1}(f(\mathbf{x}) = y) + \mathbb{1}(f(\mathbf{x}) \neq y))] \\
&= 1 - \mathbb{E}_{(\mathbf{x}, y) \sim \mathcal{D}} [\mathbb{1}(f(\mathbf{x}_{\text{hyp}}) \neq y) \cdot \mathbb{1}(f(\mathbf{x}) \neq y)] \\
&= 1 - \mathbb{E}_{(\mathbf{x}, y) \sim \mathcal{D}} [\mathbb{1}(f(\mathbf{x}) \neq y)] \cdot \mathbb{E}_{(\mathbf{x}, y) \sim \mathcal{D}_f^-} [\mathbb{1}(f(\mathbf{x}_{\text{hyp}}) \neq y)] \\
&= 1 - \mathbb{E}_{(\mathbf{x}, y) \sim \mathcal{D}} [\mathbb{1}(f(\mathbf{x}) \neq y)] \cdot \mathbb{E}_{(\mathbf{x}, y) \sim \mathcal{D}_f^-} [1 - \mathbb{1}(f(\mathbf{x}_{\text{hyp}}) = y)] \\
&= 1 - \mathbb{E}_{(\mathbf{x}, y) \sim \mathcal{D}} [\mathbb{1}(f(\mathbf{x}) \neq y)] \cdot \mathbb{E}_{(\mathbf{x}, y) \sim \mathcal{D}_f^-} [1 - \mathbb{1}(f(\mathbf{x}_{\text{hyp}}) = y)] \\
&= 1 - \mathcal{R}_{\text{nat}}(f, \mathcal{D}) \cdot (1 - \mathcal{R}_{\text{hyp}}(f, \mathcal{D}_f^-)) \\
&= 1 - (1 - \mathcal{R}_{\text{hyp}}(f, \mathcal{D}_f^-)) \cdot \mathcal{R}_{\text{nat}}(f, \mathcal{D})
\end{aligned}$$

□

### C.3 Proof of Theorem 4.5

**Lemma C.1.**  $\mathcal{R}_{\text{hyp}}(f_{\theta}, \mathcal{D}_{f_{\theta}}^-) \leq \overline{\mathcal{R}}_{\text{hyp}}(f_{\theta}, \mathcal{D}_{f_{\theta}}^-) \leq \mathcal{R}_{\text{sta}}(f, \mathcal{D}_{f_{\theta}}^-)$ , where  $\overline{\mathcal{R}}_{\text{hyp}}(f_{\theta}, \mathcal{D}_{f_{\theta}}^-) = \mathbb{E}_{(\mathbf{x}, y) \sim \mathcal{D}_{f_{\theta}}^-} [\mathbb{1}(f_{\theta}(\mathbf{x}_{\text{hyp}}) \neq f_{\theta}(\mathbf{x}))]$  and  $\mathbf{x}_{\text{hyp}} = \arg \max_{\|\mathbf{x}' - \mathbf{x}\| \leq \epsilon} \mathbb{1}(f_{\theta}(\mathbf{x}') = y)$ .

*Proof.* For the sake of brevity, here we use the notation  $f$  to represent  $f_{\theta}$ . Remember that  $f(\mathbf{x}) \neq y$  for any  $(\mathbf{x}, y) \sim \mathcal{D}_f^-$ . For the first inequality  $\mathcal{R}_{\text{hyp}}(f, \mathcal{D}_f^-) \leq \overline{\mathcal{R}}_{\text{hyp}}(f, \mathcal{D}_f^-)$ , we have

$$\begin{aligned} \mathcal{R}_{\text{hyp}}(f, \mathcal{D}_f^-) &= \mathbb{E}_{(\mathbf{x}, y) \sim \mathcal{D}_f^-} \left[ \max_{\|\mathbf{x}' - \mathbf{x}\| \leq \epsilon} \mathbb{1}(f(\mathbf{x}') = y) \right] \\ &= \mathbb{E}_{(\mathbf{x}, y) \sim \mathcal{D}_f^-} [\mathbb{1}(f(\mathbf{x}_{\text{hyp}}) = y)] \\ &\leq \mathbb{E}_{(\mathbf{x}, y) \sim \mathcal{D}_f^-} [\mathbb{1}(f(\mathbf{x}_{\text{hyp}}) \neq f(\mathbf{x}))], \end{aligned}$$

where the above inequality involves two conditions:

$$\mathbb{1}(f(\mathbf{x}_{\text{hyp}}) = y) = \begin{cases} 1 & = \mathbb{1}(f(\mathbf{x}_{\text{hyp}}) \neq f(\mathbf{x})), & \text{if } f(\mathbf{x}_{\text{hyp}}) = y, \\ 0 & \leq \mathbb{1}(f(\mathbf{x}_{\text{hyp}}) \neq f(\mathbf{x})), & \text{if } f(\mathbf{x}_{\text{hyp}}) \neq y. \end{cases}$$

For the second inequality  $\overline{\mathcal{R}}_{\text{hyp}}(f, \mathcal{D}_f^-) \leq \mathcal{R}_{\text{sta}}(f, \mathcal{D}_f^-)$ , we have

$$\begin{aligned} \overline{\mathcal{R}}_{\text{hyp}}(f, \mathcal{D}_f^-) &= \mathbb{E}_{(\mathbf{x}, y) \sim \mathcal{D}_f^-} [\mathbb{1}(f(\mathbf{x}_{\text{hyp}}) \neq f(\mathbf{x}))] \\ &\leq \mathbb{E}_{(\mathbf{x}, y) \sim \mathcal{D}_f^-} \left[ \max_{\|\mathbf{x}' - \mathbf{x}\| \leq \epsilon} \mathbb{1}(f(\mathbf{x}') \neq f(\mathbf{x})) \right], \end{aligned}$$

where the above inequality involves two conditions:

$$\mathbb{1}(f(\mathbf{x}_{\text{hyp}}) \neq f(\mathbf{x})) = \begin{cases} 1 & = \max_{\|\mathbf{x}' - \mathbf{x}\| \leq \epsilon} \mathbb{1}(f(\mathbf{x}') \neq f(\mathbf{x})), & \text{if } f(\mathbf{x}_{\text{hyp}}) = y, \\ 0 & \leq \max_{\|\mathbf{x}' - \mathbf{x}\| \leq \epsilon} \mathbb{1}(f(\mathbf{x}') \neq f(\mathbf{x})), & \text{if } f(\mathbf{x}_{\text{hyp}}) \neq y. \end{cases}$$

□

**Theorem 4.5 (restated).**  $\mathcal{R}_{\text{sta}}(f_{\theta}, \mathcal{D}) = (1 - \mathcal{R}_{\text{nat}}(f_{\theta}, \mathcal{D})) \cdot \mathcal{R}_{\text{adv}}(f_{\theta}, \mathcal{D}_{f_{\theta}}^+) + \mathcal{R}_{\text{nat}}(f_{\theta}, \mathcal{D}) \cdot \mathcal{R}_{\text{sta}}(f_{\theta}, \mathcal{D}_{f_{\theta}}^-)$ , where we have  $\mathcal{R}_{\text{sta}}(f_{\theta}, \mathcal{D}_{f_{\theta}}^-) \geq \mathcal{R}_{\text{hyp}}(f_{\theta}, \mathcal{D}_{f_{\theta}}^-)$ .

*Proof.* For the sake of brevity, here we use the notation  $f$  to represent  $f_\theta$ .

$$\begin{aligned}
\mathcal{R}_{\text{sta}}(f, \mathcal{D}) &= \mathbb{E}_{(\mathbf{x}, y) \sim \mathcal{D}} \left[ \max_{\|\mathbf{x}' - \mathbf{x}\| \leq \epsilon} \mathbb{1}(f(\mathbf{x}') \neq f(\mathbf{x})) \right] \\
&= \mathbb{E}_{(\mathbf{x}, y) \sim \mathcal{D}} \left[ \max_{\|\mathbf{x}' - \mathbf{x}\| \leq \epsilon} \mathbb{1}(f(\mathbf{x}') \neq f(\mathbf{x})) \cdot 1 \right] \\
&= \mathbb{E}_{(\mathbf{x}, y) \sim \mathcal{D}} \left[ \max_{\|\mathbf{x}' - \mathbf{x}\| \leq \epsilon} \mathbb{1}(f(\mathbf{x}') \neq f(\mathbf{x})) \cdot (\mathbb{1}(f(\mathbf{x}) = y) + \mathbb{1}(f(\mathbf{x}) \neq y)) \right] \\
&= \mathbb{E}_{(\mathbf{x}, y) \sim \mathcal{D}} \left[ \max_{\|\mathbf{x}' - \mathbf{x}\| \leq \epsilon} \mathbb{1}(f(\mathbf{x}') \neq f(\mathbf{x})) \cdot \mathbb{1}(f(\mathbf{x}) = y) \right] \\
&\quad + \mathbb{E}_{(\mathbf{x}, y) \sim \mathcal{D}} \left[ \max_{\|\mathbf{x}' - \mathbf{x}\| \leq \epsilon} \mathbb{1}(f(\mathbf{x}') \neq f(\mathbf{x})) \cdot \mathbb{1}(f(\mathbf{x}) \neq y) \right] \\
&= \mathbb{E}_{(\mathbf{x}, y) \sim \mathcal{D}} \left[ \max_{\|\mathbf{x}' - \mathbf{x}\| \leq \epsilon} \mathbb{1}(f(\mathbf{x}') \neq y) \cdot \mathbb{1}(f(\mathbf{x}) = y) \right] \\
&\quad + \mathbb{E}_{(\mathbf{x}, y) \sim \mathcal{D}} \left[ \max_{\|\mathbf{x}' - \mathbf{x}\| \leq \epsilon} \mathbb{1}(f(\mathbf{x}') \neq f(\mathbf{x})) \cdot \mathbb{1}(f(\mathbf{x}) \neq y) \right] \\
&= \mathbb{E}_{(\mathbf{x}, y) \sim \mathcal{D}} [\mathbb{1}(f(\mathbf{x}) = y)] \cdot \mathbb{E}_{(\mathbf{x}, y) \sim \mathcal{D}_f^+} \left[ \max_{\|\mathbf{x}' - \mathbf{x}\| \leq \epsilon} \mathbb{1}(f(\mathbf{x}') \neq y) \right] \\
&\quad + \mathbb{E}_{(\mathbf{x}, y) \sim \mathcal{D}} [\mathbb{1}(f(\mathbf{x}) \neq y)] \cdot \mathbb{E}_{(\mathbf{x}, y) \sim \mathcal{D}_f^-} \left[ \max_{\|\mathbf{x}' - \mathbf{x}\| \leq \epsilon} \mathbb{1}(f(\mathbf{x}') \neq f(\mathbf{x})) \right] \\
&= \mathbb{E}_{(\mathbf{x}, y) \sim \mathcal{D}} [1 - \mathbb{1}(f(\mathbf{x}) = y)] \cdot \mathbb{E}_{(\mathbf{x}, y) \sim \mathcal{D}_f^+} \left[ \max_{\|\mathbf{x}' - \mathbf{x}\| \leq \epsilon} \mathbb{1}(f(\mathbf{x}') \neq y) \right] \\
&\quad + \mathbb{E}_{(\mathbf{x}, y) \sim \mathcal{D}} [\mathbb{1}(f(\mathbf{x}) \neq y)] \cdot \mathbb{E}_{(\mathbf{x}, y) \sim \mathcal{D}_f^-} \left[ \max_{\|\mathbf{x}' - \mathbf{x}\| \leq \epsilon} \mathbb{1}(f(\mathbf{x}') \neq f(\mathbf{x})) \right] \\
&= (1 - \mathcal{R}_{\text{nat}}(f, \mathcal{D})) \cdot \mathcal{R}_{\text{adv}}(f, \mathcal{D}_f^+) + \mathcal{R}_{\text{nat}}(f, \mathcal{D}) \cdot \mathcal{R}_{\text{sta}}(f, \mathcal{D}_f^-)
\end{aligned}$$

Then, by combining Lemma C.1, we have  $\mathcal{R}_{\text{sta}}(f_\theta, \mathcal{D}_{f_\theta}^-) \geq \mathcal{R}_{\text{hyp}}(f_\theta, \mathcal{D}_{f_\theta}^-)$ .  $\square$

#### C.4 Proof of Corollary G.1

Zhang et al. (2021a) showed that  $\ell_\infty$ -dist nets are 1-Lipschitz with respect to  $\ell_\infty$ -norm, which is a nice theoretical property in controlling the robustness of the model.

**Fact C.2.** (Fact 3.4 in Zhang et al. (2021a)) Any  $\ell_\infty$ -dist net  $\mathbf{g}(\cdot)$  is 1-Lipschitz with respect to  $\ell_\infty$ -norm, i.e., for any  $\mathbf{x}_1, \mathbf{x}_2 \in \mathbb{R}^d$ , we have  $\|\mathbf{g}(\mathbf{x}_1) - \mathbf{g}(\mathbf{x}_2)\|_\infty \leq \|\mathbf{x}_1 - \mathbf{x}_2\|_\infty$ .

Since  $\mathbf{g}$  is 1-Lipschitz with respect to  $\ell_\infty$ -norm, if the perturbation over  $\mathbf{x}$  is rather small, the change of the output can be bounded and the predication of the perturbed data  $\mathbf{x}'$  will not change to  $y$  as long as  $\max_i g_i(\mathbf{x}') > g_y(\mathbf{x}')$ , which directly bounds the certified hypocritical risk.

**Corollary G.1 (restated).** Given the  $\ell_\infty$ -dist net  $f(\mathbf{x}) = \arg \max_{i \in [M]} g_i(\mathbf{x})$  defined in Eq. 4 and the distribution of misclassified examples  $\mathcal{D}_f^-$  with respect to  $f$ , we have

$$\mathcal{R}_{\text{hyp}}(f, \mathcal{D}_f^-) \leq \mathbb{E}_{(\mathbf{x}, y) \sim \mathcal{D}_f^-} [\mathbb{1}(\max_i g_i(\mathbf{x}) - g_y(\mathbf{x}) < 2\epsilon)].$$

*Proof.* Firstly, similar to the robust radius (Zhai et al. 2020; Zhang et al. 2021a), we define the *hypocritical radius* as:

$$\text{HR}(f; \mathbf{x}, y) = \inf_{f(\mathbf{x}') = y} \|\mathbf{x}' - \mathbf{x}\|_\infty,$$

which represents the minimal radius required to correct model prediction. Exactly computing the the hypocritical radius of a classifier induced by a standard deep neural network is very difficult. Next we seek to derive a tight lower bound of  $\text{HR}(f; \mathbf{x}, y)$  using the  $\ell_\infty$ -dist net. Considering a misclassified example  $\mathbf{x}$  such that  $f(\mathbf{x}) \neq y$ , we define  $\text{margin}(f; \mathbf{x}, y)$  as the difference between the largest and the  $y$ -th elements of  $\mathbf{g}(\mathbf{x})$ :

$$\text{margin}(f; \mathbf{x}, y) = \max_i g_i(\mathbf{x}) - g_y(\mathbf{x}).$$

Then for any  $\mathbf{x}'$  satisfying  $\|\mathbf{x} - \mathbf{x}'\|_\infty < \text{margin}(f; \mathbf{x}, y)/2$ , each element of  $\mathbf{g}(\mathbf{x})$  can move at most  $\text{margin}(f; \mathbf{x}, y)/2$  when  $\mathbf{x}$  changes to  $\mathbf{x}'$  due to that  $\mathbf{g}(\mathbf{x})$  is 1-Lipschitz. Therefore,  $g_y(\mathbf{x}')$  cannot be the largest element of  $\mathbf{g}(\mathbf{x}')$ , that is,  $f(\mathbf{x}') \neq y$ . In other words,  $\text{margin}(f; \mathbf{x}, y)/2$  is a provable lower bound of the hypocritical radius:  $\text{margin}(f; \mathbf{x}, y)/2 \leq \text{HR}(f; \mathbf{x}, y)$ .

This certified radius leads to a guaranteed upper bound of the hypocritical risk:

$$\max_{\|\mathbf{x}' - \mathbf{x}\|_\infty \leq \epsilon} \mathbb{1}(f(\mathbf{x}') = y) \leq \mathbb{1}(\text{margin}(f; \mathbf{x}, y)/2 < \epsilon),$$

i.e., an example can be perturbed to be classified only if the difference between  $\max_i g_i(\mathbf{x})$  and  $g_y(\mathbf{x})$  is less than  $\epsilon$ . The expectation of the above inequality over  $\mathcal{D}_f^-$  serves as a performance metric of the provable hypocritical robustness:

$$\mathbb{E}_{(\mathbf{x}, y) \sim \mathcal{D}_f^-} \left[ \max_{\|\mathbf{x}' - \mathbf{x}\|_\infty \leq \epsilon} \mathbb{1}(f(\mathbf{x}') = y) \right] \leq \mathbb{E}_{(\mathbf{x}, y) \sim \mathcal{D}_f^-} \left[ \mathbb{1}(\max_i g_i(\mathbf{x}) - g_y(\mathbf{x}) < 2\epsilon) \right].$$

□

## D Crafting Hypocritical Data via Various Attacks

In addition to the PGD attack adopted in the main text, many other techniques (such as FGSM (Goodfellow, Shlens, and Szegedy 2015) and C&W (Carlini and Wagner 2017)) that were developed for crafting adversarial examples can also be used for the current study of hypocritical attacks. To support this claim, we adaptively modify their objective function to craft hypocritical examples. Results on CIFAR-10 are summarized in Table 14, where PGD-20/100 denotes the PGD attack with 20/100 iterations, and C&W-100 is similar. We observe that for hypocritical attacks: *i*) FGSM is relatively weak, *ii*) PGD-100 is slightly stronger than PGD-20, and *iii*) C&W is slightly better than PGD. These phenomena are similar to the case of adversarial examples, indicating that future work may easily adapt more advanced techniques, such as AutoAttack (Croce and Hein 2020), to further boost hypocritical attacks.

Table 14: Verification accuracy (%) of ResNet-18 models under  $\ell_\infty$  threat model across various attack techniques. Here, the THRM model is trained with  $\lambda = 40$ , whose clean accuracy is comparable to the TRADES model with  $\lambda = 6$ .

Model	Clean	FGSM	PGD-20	PGD-100	C&W-100
Naive	8.46	28.29	82.56	84.24	<b>88.23</b>
Quality (NT)	94.38	99.60	<b>100.00</b>	<b>100.00</b>	<b>100.00</b>
Quality (PGD-AT)	84.08	88.96	96.92	96.95	<b>97.29</b>
Quality (TRADES)	81.05	86.28	95.17	95.19	<b>96.08</b>
Quality (THRM)	81.19	86.10	94.18	94.20	<b>95.13</b>

## E Trade-off between Risks

### E.1 Example 1

Motivated by the trade-off between natural risk and adversarial risk (Tsipras et al. 2019; Zhang et al. 2019), we notice that there may also exist a tension between the goal of natural risk minimization and hypocritical risk minimization. To illustrate the phenomenon, similar to the toy example in Zhang et al. (2019), we provide another toy example here.

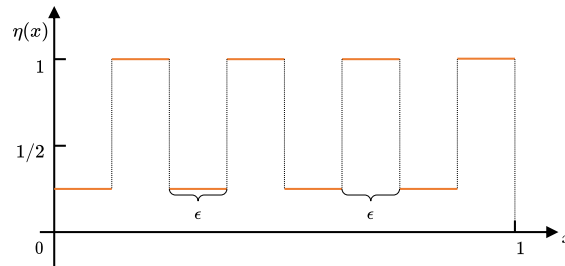


Figure 8: Visualization of  $\eta(x)$ .

Consider the case  $(x, y) \in \mathbb{R} \times \{-1, +1\}$  from a distribution  $\mathcal{D}$ , where the marginal distribution over the instance space is a uniform distribution over  $[0, 1]$ , and for  $k = 0, 1, \dots, \lceil \frac{1}{2\epsilon} - 1 \rceil$ ,

$$\begin{aligned} \eta(x) &= \Pr(y = +1 \mid x) \\ &= \begin{cases} 1/4, & x \in [2k\epsilon, (2k+1)\epsilon), \\ 1, & x \in ((2k+1)\epsilon, (2k+2)\epsilon]. \end{cases} \end{aligned}$$



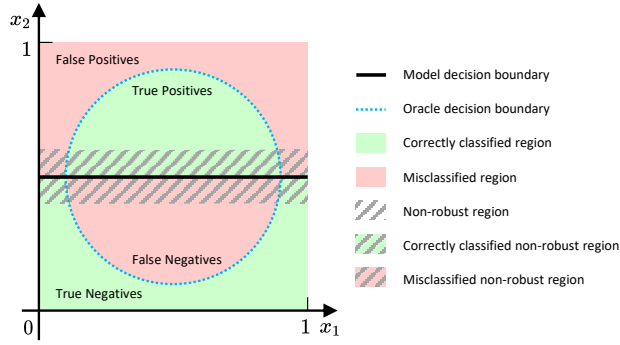


Figure 9: Visualization of decision boundary for oracle and model.

See Figure 8 for visualization of  $\eta(x)$ . We consider two classifiers: a) the Bayes optimal classifier  $\text{sign}(2\eta(x) - 1)$ ; b) the all-one classifier which always outputs “positive”. Table 15 displays the trade-off between the natural risk and the hypocritical risk on misclassified examples: the minimal natural risk is achieved by the Bayes optimal classifier with large hypocritical risk, while the minimal hypocritical risk is achieved by the all-one classifier with large natural risk.

Table 15: Comparison of Bayes optimal classifier and all-one classifier.

	Bayes Optimal Classifier	All-One Classifier
$\mathcal{R}_{\text{nat}}(f, \mathcal{D})$	1/8 (optimal)	3/8
$\mathcal{R}_{\text{hyp}}(f, \mathcal{D})$	1	5/8
$\mathcal{R}_{\text{adv}}(f, \mathcal{D})$	1	3/8
$\mathcal{R}_{\text{hyp}}(f, \mathcal{D}_f^-)$	1	0 (optimal)
$\mathcal{R}_{\text{adv}}(f, \mathcal{D}_f^+)$	1	0 (optimal)

## E.2 Example 2

In Example 1, the optimal solution for adversarial risk and hypocritical risk is the same by coincidence. Next, we show that the minimizers of natural risk and hypocritical risk are not necessarily consistent by providing the second toy example, which is motivated by the well-known trade-off between precision and recall (Buckland and Gey 1994).

Consider the case  $(x, y) \in \mathbb{R}^2 \times \{-1, +1\}$  from a distribution  $\mathcal{D}$ , where the marginal distribution over the instance space is a uniform distribution over  $[0, 1]^2$ . Let the decision boundary of the oracle (ground truth) be a circle:

$$\mathcal{O}(x) = \text{sign}(r - \|x - c\|_2),$$

where the center  $c = (0.5, 0.5)^\top$  and the radius  $r = 0.4$ . The points inside the circle are labeled as belonging to the positive class, otherwise they are labeled as belonging to the negative class. We consider the linear classifier  $f$  with fixed  $w = (0, 1)^\top$  and a tunable threshold  $b$ :

$$f(x) = \text{sign}(w^\top x - b) = \text{sign}(x_2 - b).$$

See Figure 9 for visualization of decision boundary for the oracle and the linear classifier over the instance space. Here we choose the  $l_2$ -norm with  $\epsilon = 0.1$  as the threat model. We tune the threshold  $b$  of the classifier over  $[0, 1]$  to show the trade-off between metrics. The computation of the metrics is visualized in Figure 10. Precision is the number of true positives divided by the the sum of true positives and false positives. Recall is the number of true positives divided by the sum of true positives and false negatives. We compare the adversarial risk on correctly classified examples and the hypocritical risk on misclassified examples.

Figure 11 plots the curve of precision and recall versus the threshold  $b$ . As we can see, there is a explicit precision-recall tradeoff between the two gray dotted lines. Similarly, Figure 12 plots the curve of  $\mathcal{R}_{\text{adv}}(f, \mathcal{D}_f^+)$  and  $\mathcal{R}_{\text{hyp}}(f, \mathcal{D}_f^-)$  versus the threshold  $b$ . As we can see, the tradeoff exists almost everywhere: as the adversarial risk increases, the hypocritical risk decreases, and vice versa.



Figure 10: Visualization of formulation for precision, recall, adversarial risk, and hypocritical risk. These metrics can be viewed as the ratio of specific areas in the section example.

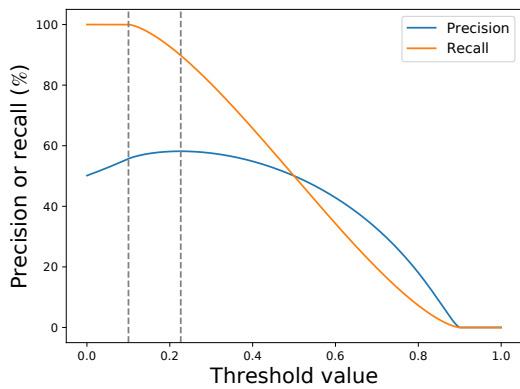


Figure 11: The tradeoff between precision and recall in the section example.

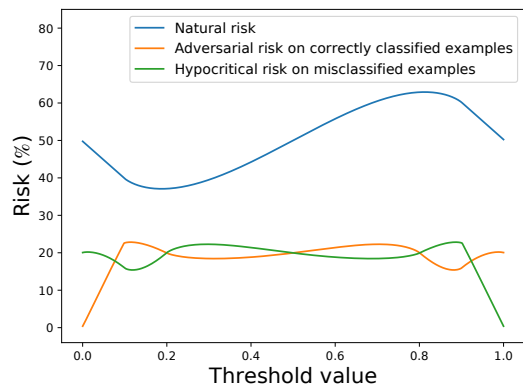


Figure 12: The tradeoff between risks in the section example.

## F Details on THRM

In this section, we derive the objective of THRM in Eq. (3) from the theoretical perspective.

As a by-product of Lemma C.1, we get a tighter upper bound of the hypocritical risk on misclassified examples, i.e.,  $\overline{\mathcal{R}}_{\text{hyp}}(f_\theta, \mathcal{D}_{f_\theta}^-)$  defined in Lemma C.1. Similar to TRADES, we propose to minimize the composition of the natural risk and this tighter upper bound:  $\mathcal{R}_{\text{nat}}(f_\theta, \mathcal{D}) + \lambda \overline{\mathcal{R}}_{\text{hyp}}(f_\theta, \mathcal{D}_{f_\theta}^-)$ . However, optimization over the 0-1 loss is intractable in practice. Inspired by Madry et al. (2018); Zhang et al. (2019); Wang et al. (2020b), we also seek for proper surrogate loss functions which are computationally tractable. Specifically, we adopt the commonly used cross entropy (CE) loss as the surrogate loss for the indicator function  $\mathbb{1}(f_\theta(\mathbf{x}) \neq y)$  in the natural risk. Further, observed that  $\overline{\mathcal{R}}_{\text{hyp}}(f_\theta, \mathcal{D}_{f_\theta}^-) = (1/\mathcal{R}_{\text{nat}}(f_\theta, \mathcal{D})) \cdot \mathcal{R}_{\text{hyp}}(f_\theta, \mathcal{D})$ , we absorb the term  $\mathcal{R}_{\text{nat}}(f_\theta, \mathcal{D})$  into  $\lambda$ , and similarly use the KL divergence as the surrogate loss (Zheng et al. 2016; Zhang et al. 2019; Wang et al. 2020b) for the indicator function  $\mathbb{1}(f_\theta(\mathbf{x}_{\text{hyp}}) \neq f_\theta(\mathbf{x}))$ . Based on the surrogate loss functions, we can state the final objective function for the adaptive robust training method:

$$\mathcal{L}_{\text{THRM}} = \mathbb{E}_{(\mathbf{x}, y) \sim \mathcal{D}} [\text{CE}(\mathbf{p}_\theta(\mathbf{x}), y) + \lambda \cdot \text{KL}(\mathbf{p}_\theta(\mathbf{x}) \parallel \mathbf{p}_\theta(\mathbf{x}_{\text{hyp}}))],$$

where  $\mathbf{x}_{\text{hyp}}$  is approximately generated by minimizing the CE loss using PGD as in Section 3. The first term in the above objective is the standard loss that maximizes the natural accuracy. The second term is also physically meaningful, which forces the predictive distributions of clean examples and hypocritical examples to be similar to each other, and thus encourages the model to robustly predict its failures on hypocritical examples.

We name the method THRM (Trade-off for Hypocritical Risk Minimization). This is largely because we notice that, similar to the trade-off between the natural risk and the adversarial risk (Tsipras et al. 2019; Zhang et al. 2019), the minimizers of the natural risk and the hypocritical risk are not necessarily consistent. Training models to be robust against hypocritical perturbations may lead to a reduction of natural accuracy. We illustrated this phenomenon by constructing toy examples in Appendix E.

## G Details on $\ell_\infty$ -dist Nets

In Section 5.2, we empirically computed the hypocritical risk achieved by the PGD-based attack, which is actually a lower bound of the true hypocritical risk. This means that more hypocritical examples may be constructed by stronger hypocritical attacks. Unfortunately, exactly computing the true hypocritical risk for a standard DNN is very difficult, since computing the  $\ell_p$  robust radius of a DNN is NP-hard (Katz et al. 2017). Therefore, we turn to seek for a tight upper bound of the true hypocritical risk. Similar to the definition of certified adversarial risk in previous works (Raghunathan, Steinhardt, and Liang 2018; Wong and Kolter 2018; Weng et al. 2018; Zhang et al. 2018; Gowal et al. 2019; Salman et al. 2019; Boopathy et al. 2019; Dathathri et al. 2020; Xu et al. 2021), we define the *certified hypocritical risk* as a provable upper bound on the achievable hypocritical risk by *any* hypocritical attack.

Next, we exemplify the certified hypocritical risk using a recent state-of-the-art certification method called  $\ell_\infty$ -dist nets (Zhang et al. 2021a), which inherently resist  $\ell_\infty$  perturbations by using  $\ell_\infty$ -distance as the basic operation. An  $L$  layer  $\ell_\infty$ -dist net is defined as  $f(\mathbf{x}) = \arg \max_{i \in [M]} g_i(\mathbf{x})$ , in which

$$\mathbf{g}(\mathbf{x}) = (-x_1^{(L)}, -x_2^{(L)}, \dots, -x_M^{(L)}), x_k^{(l)} = \|\mathbf{x}^{l-1} - \mathbf{w}^{(l,k)}\|_\infty + b^{(l,k)}, 1 \leq l \leq L, 1 \leq k \leq d_l, \quad (4)$$

where  $d_l$  is the number of units in the  $l$ -th layer,  $\mathbf{x}^{(0)} = \mathbf{x}$  is the input,  $\mathbf{x}^l = (x_1^{(l)}, x_2^{(l)}, \dots, x_{d_l}^{(l)})$  is the output of the  $l$ -th layer,  $\mathbf{w}^{(l,k)}$  and  $b^{(l,k)}$  is the parameters of the  $k$ -th unit in the  $l$ -th layer.

The following corollary allows us to make use of the  $\ell_\infty$ -dist net to certify the hypocritical risk:

**Corollary G.1.** *Given the  $\ell_\infty$ -dist net  $f(\mathbf{x}) = \arg \max_{i \in [M]} g_i(\mathbf{x})$  defined in Eq. 4 and the distribution of misclassified examples  $\mathcal{D}_f^-$  with respect to  $f$ , we have*

$$\mathcal{R}_{\text{hyp}}(f, \mathcal{D}_f^-) \leq \mathbb{E}_{(\mathbf{x}, y) \sim \mathcal{D}_f^-} [\mathbb{1}(\max_i g_i(\mathbf{x}) - g_y(\mathbf{x}) < 2\epsilon)].$$

The proof is provided in Appendix C.4, which utilizes the 1-Lipschitz property of  $\ell_\infty$ -dist nets to guarantee the upper bound on the hypocritical risk. Using this bound, we can certify the hypocritical risk of an  $\ell_\infty$ -dist net under  $\ell_\infty$ -norm perturbations with little computational cost (only one forward pass for each example). Following the implementation in Zhang et al. (2021a), we use a 6-layer  $\ell_\infty$ -dist net for CIFAR-10. Other configurations and hyper-parameters are also the same as the original paper.

Results of the models trained on the *Quality* data and the *Poisoning* data are summarized in Table 16. We report both the empirical hypocritical risk achieved by the PGD-based attack and the certified hypocritical risk guaranteed by Corollary G.1. The former is naturally lower than the latter. The true hypocritical risk will exist between the empirical and certified hypocritical risks. For completeness, we additionally report the certified adversarial (hypocritical) accuracy, which is a strict lower bound (upper bound) on the achievable accuracy by any adversarial (hypocritical) attack.

As can be seen from Table 16, the  $\ell_\infty$ -dist net achieves moderate certified hypocritical risk. For both the *Quality* model and the *Poisoning* model, nearly half of the errors are guaranteed not to be covered up by any attack. On the other hand, the  $\ell_\infty$ -dist

Table 16: Empirical and certified accuracy (%) / risk (%) of  $\ell_\infty$ -dist nets on CIFAR-10 under  $\ell_\infty$  threat model.  $\mathcal{D}$ ,  $\mathcal{A}$ , and  $\mathcal{F}$  denote the model accuracy evaluated on clean examples, adversarially perturbed examples, and hypocritically perturbed examples, respectively.  $\mathcal{R}_{\text{nat}}$  and  $\mathcal{R}_{\text{hyp}}$  denote the natural risk and the hypocritical risk on misclassified examples, respectively.

Model	$\mathcal{D}$	$\mathcal{A}$		$\mathcal{F}$		$\mathcal{R}_{\text{nat}}$	$\mathcal{R}_{\text{hyp}}$	
		Empirical	Certified	Empirical	Certified		Empirical	Certified
Poisoning	55.62	36.36	31.87	76.57	83.36	44.38	47.25	62.51
Quality	56.66	37.24	32.79	77.06	83.86	43.34	47.07	62.76

net seems to perform worse than TRADES and THRM in terms of empirical hypocritical risk. For example, when training on the CIFAR-10 *Quality* data, the  $\ell_\infty$ -dist net has 43.34% natural risk and 47.07% empirical hypocritical risk; for comparison, TRADES with  $\lambda = 80$  achieves 33.47% natural risk and 40.99% empirical hypocritical risk. Thus, the certified robustness against hypocritical perturbations is barely satisfactory; in particular, the PGD-based attack can already conceal almost half of the errors, and perhaps more powerful attacks can conceal more than half of the errors. Other advanced techniques (such as designing more effective architectures (Huang et al. 2021b), more principled initializations (Shi et al. 2021), and combination with other certification methods (Zhang et al. 2020a)) may help to achieve a better certified hypocritical risk. We leave this as future work.